

Stephen F. Austin State University

SFA ScholarWorks

Electronic Theses and Dissertations

Summer 8-17-2019

2-D and 3-D Temporal Modeling of Solute Migration through Low Permeable Media using Electrical Resistivity, Nacogdoches County, Texas

Kaleb Henry
henryk@jacks.sfasu.edu

Kevin W. stafford
staffordk@sfasu.edu

Wesley Brown
brownwa1@sfasu.edu

Melinda Faulkner
mgshaw@sfasu.edu

Matthew McBroom
mcbroommatth@sfasu.edu

Follow this and additional works at: <https://scholarworks.sfasu.edu/etds>



Part of the [Earth Sciences Commons](#)

[Tell us](#) how this article helped you.

Repository Citation

Henry, Kaleb; stafford, Kevin W.; Brown, Wesley; Faulkner, Melinda; and McBroom, Matthew, "2-D and 3-D Temporal Modeling of Solute Migration through Low Permeable Media using Electrical Resistivity, Nacogdoches County, Texas" (2019). *Electronic Theses and Dissertations*. 251.
<https://scholarworks.sfasu.edu/etds/251>

This Thesis is brought to you for free and open access by SFA ScholarWorks. It has been accepted for inclusion in Electronic Theses and Dissertations by an authorized administrator of SFA ScholarWorks. For more information, please contact cdsscholarworks@sfasu.edu.

2-D and 3-D Temporal Modeling of Solute Migration through Low Permeable Media using Electrical Resistivity, Nacogdoches County, Texas

Creative Commons License



This work is licensed under a [Creative Commons Attribution-Noncommercial-No Derivative Works 4.0 License](https://creativecommons.org/licenses/by-nc-nd/4.0/).

**2-D and 3-D Temporal Modeling of Solute Migration through Low Permeable Media using
Electrical Resistivity, Nacogdoches County, Texas**

By

Kaleb J. Henry, Bachelor of Science

Presented to the Faculty of the Graduate School of

Stephen F. Austin State University

In Partial Fulfillment

Of the Requirements

For the Degree of

Master of Science

STEPHEN F. AUSTIN STATE UNIVERSITY

(August 2019)

**2-D and 3-D Temporal Modeling of Solute Migration through Low Permeable Media using
Electrical Resistivity, Nacogdoches County, Texas**

By

KALEB J. HENRY, Bachelor of Science

APPROVED:

Dr. Kevin Stafford, Thesis Director

Dr. Wesley Brown, Committee Member

Dr. Melinda Faulkner, Committee Member

Dr. Matthew McBroom, Committee Member

Pauline M. Sampson, Ph.D.
Dean of Research and Graduate Studies

ABSTRACT

The Reklaw Formation is the upper bounding unit for the Carrizo-Wilcox Aquifer throughout the Gulf Coastal Plain of East Texas and consists of low permeability, glauconite-rich strata that isolate semi-confined portions of the aquifer system from potential contaminants. Electrical resistivity methods were employed within a forested watershed in Nacogdoches County, Texas to characterize solute transport. 2-D and 3-D temporal resistivity data collected with an AGI SuperSting (R8/IP) were processed with AGI Earthimager 2D/3D software for inversion modeling. Data were collected over 135 days within a 14 X 26 meter (46 X 85 feet) gridded survey at 15-day intervals after initiation of a NaCl solute plume; numerical modeling was developed from physical site characterizations.

Resistivity analyses and numerical modeling demonstrated solute migration is extremely slow within the Reklaw Formation, confirming strata effectiveness for preventing contaminant migration into the Carrizo-Wilcox Aquifer. Numerical modeling indicated rapid solute dilution with migration dominated by diffusion. 2-D inversion modeling confirmed dominance of solute diffusion, but clearly identified macropore heterogeneity that increased advection transport; 3-D inversion modeling proved relatively ineffective. This study demonstrates the effectiveness of electrical resistivity

characterization for delineating heterogenic and anisotropic controls on solute migration that are often poorly defined in simple numerical modeling.

ACKNOWLEDGEMENTS

Without the help of my thesis advisor, Dr. Kevin Stafford, this study would not have been possible. I am also thankful for the Geology Department and the members of my committee who took the time to assist me in data collection and completion of this manuscript: Dr. Wesley Brown, Dr. Melinda Faulkner, and Dr. Mathew McBroom. I would also like to thank my family, friends, and colleagues for supporting me through this research.

TABLE OF CONTENTS

ABSTRACT	i
ACKNOWLEDGEMENTS.....	iii
TABLE OF CONTENTS.....	iv
LIST OF FIGURES	vi
LIST OF TABLES.....	viii
LIST OF EQUATIONS	ix
PREFACE	x
2-D AND 3-D TEMPORAL MODELING OF SOLUTE MIGRATION THROUGH LOW PERMEABLE MEDIA USING ELECTRICAL RESISTIVITY METHODS, NACOGDOCHES COUNTY, TEXAS.....	1
ABSTRACT.....	1
INTRODUCTION.....	3
STUDY AREA	7
ELECTRICAL RESISTIVITY METHODS	13
NUMERICAL MODELING METHODS.....	15
RESULTS AND DISCUSSION	21
3-D RESISTIVITY ANALYSIS.....	24
3-D: 15-Day Survey	26

3-D: 45-Day Survey	26
3-D: 105-Day Survey	27
2-D ANALYSES AND NUMERICAL MODELING.....	29
2-D: 15-Day Analyses.....	29
2-D: 45-Day Analyses.....	32
2-D: 75-Day Analyses.....	33
2-D: 105-Day Analyses.....	34
2-D: 135-Day Analyses.....	35
CONCLUSIONS.....	36
REFERENCES.....	41
APPENDIX A.....	45
VITA.....	75

LIST OF FIGURES

- Figure 1. Location of the study area within the Reklaw Formation in Nacogdoches County, Texas. Outcrop area of Reklaw Formation is shown in red; study site is represented by the star east of Nacogdoches, Texas. ...6
- Figure 2. Stratigraphic column of the Claiborne Group. Aquifer bearing horizons highlighted in blue (modified from Watkins, 2018; Fisher, 1964; Forestar, 2011).8
- Figure 3. Temperature (maximum and minimum) and precipitation variations within the region of the study area from the month of June to December. Blue dots are indicating the days at which both 3-D and 2-D electrical resistivity measurements were recorded.....12
- Figure 4. Plan view of the study site showing location of each piezometer, soil coring, and infiltration test conducted, as well as the location for every other electrode labeled within the 3-D resistivity array.....17
- Figure 5. Particle-size distribution, porosity, and hydraulic conductivity values from ground level to 250 cm (98 in) deep for sediment core sampling proximal to solute introduction location. Hydraulic conductivity values in graph are measured in cm/sec.22
- Figure 6. Dynamic slices of 3-D inverted resistivity models: A) Initial background survey (Day 1) (RMS = 8.8%, L2 norm = 1.1, iteration = 8); B) 15-day survey (RMS = 6.9%, L2 norm = 1.0, iteration = 8); C) 45-day survey (RMS = 2.8%, L2 norm = 0.2, iteration = 8); D) 105-day survey (RMS = 2.2%, L2 norm = 0.8, iteration = 8).25
- Figure 7. 2-D inverted electrical resistivity sections: A) 15-day survey (RMS error = 2.57%, L2 norm = 0.73, iteration = 8); B) 45-day survey (RMS error = 2.44%, L2 norm = 0.65, iteration = 8); C) 75-day survey (RMS = 2.91%, L2 norm = 0.93, iteration = 8); D) 105-day survey (RMS = 2.24%, L2 norm = 0.55, iteration = 8); E) 135-day survey (RMS = 3.66%, L2 norm = 1.22, iteration = 8).30

Figure 8. Refined inverted resistivity sections (left) with associated numerical model (right): A) 15-day survey (RMS error = 1.46%, L2 norm = 0.24, Iteration = 8.); B) 45-day survey (RMS error = 2.09%, L2 norm = 0.48, Iteration = 8.); C) 75-day Survey (RMS error = 1.98%, L2 norm = 0.36, Iteration = 8.); D) 105-day survey (RMS error = 1.82%, L2 norm = 0.37, Iteration = 8.); E) 135-day survey (RMS error = 1.79%, L2 norm = 0.32, Iteration = 8).31

LIST OF TABLES

Table A-1. Slug tests administered to each well, including the data, the amount of water delivered, and the rate at which the well recovered (cm/sec).....	67
Table A-2. Infiltration tests conducted in four locations and represented by J1, J2, J3, and J4.	68
Table A-3. Particle size analysis conducted on sediments located at site 1 (close to “injection” site).	69
Table A-4. Particle size analysis conducted on sediments located at site 2 (near well #1).	70
Table A-5. Particle size analysis conducted on sediments located at site 3 (near the back right of the grid).....	71
Table A-6. Particle size analysis for percentage of sand, silt, and clay. Located at site 1 (close to “injection” site).....	72
Table A-7. Particle size analysis for percentage of sand, silt, and clay. Located at site 2 (near well #1).....	73
Table A-8. Particle size analysis for percentage of sand, silt, and clay. Located at site 2 (near back right of study grid).....	74
Table A9A. Solute plume migration in each direction stemming from the “injection” site.	75
Table A9B. Solute plume migration in each direction stemming from the “injection” site.	76

LIST OF EQUATIONS

$$v_x = \frac{K}{n_e} \frac{dh}{dl} \dots\dots\dots 17$$

$$D_L = a_L v_i + D^*; D_T = a_T v_i + D^* \dots\dots\dots 18$$

$$C^* = K_d C \dots\dots\dots 18$$

$$1 + \frac{B_d}{\theta} K_d = r_f \dots\dots\dots 19$$

$$C_i(x, t) = C_0 \operatorname{erfc} \frac{x}{2(D^*t)^{0.5}} \dots\dots\dots 19$$

$$C(x, y, t) = \frac{C_0 A}{4\pi t (D_L D_T)^{0.5}} \exp \left[-\frac{((x-x_0)-v_x t)^2}{4D_L t} - \frac{(y-y_0)^2}{4D_T t} \right] \dots\dots\dots 19$$

PREFACE

The basis of this research was to characterize and delineate migration patterns of subsurface solute plumes within low permeable media. In this study, electrical resistivity and numerical modeling were the chosen method to achieve this. A secondary goal of this project was to evaluate the effectiveness of the AGI Supersting (R8/IPP) for 2-D and 3-D solute studies. This study was conducted between June and December of 2019.

The following manuscript was formatted to be submitted to the “Texas Water Journal” for publication. Additional data gathered in this study beyond the scope of prepared manuscript appears in Appendix A, including data collected, processed, and analyzed throughout the course of this investigation.

**2-D and 3-D Temporal Modeling of Solute Migration through Low Permeable Media
using Electrical Resistivity, Nacogdoches County, Texas**

ABSTRACT

The Reklaw Formation is the upper bounding unit for the Carrizo-Wilcox Aquifer throughout the Gulf Coastal Plain of East Texas and consists of low permeability, glauconite-rich strata that isolate semi-confined portions of the aquifer system from potential contaminants. Electrical resistivity methods were employed within a forested watershed in Nacogdoches County, Texas to characterize solute transport. 2-D and 3-D temporal resistivity data collected with an AGI SuperSting (R8/IP) were processed with AGI Earthimager 2D/3D software for inversion modeling. Data were collected over 135 days within a 14 X 26 meter (46 X 85 feet) gridded survey at 15-day intervals after initiation of a NaCl solute plume; numerical modeling was developed from physical site characterizations.

Resistivity analyses and numerical modeling demonstrated solute migration is extremely slow within the Reklaw Formation, confirming strata effectiveness for preventing contaminant migration into the Carrizo-Wilcox Aquifer. Numerical modeling indicated rapid solute dilution with migration dominated by diffusion. 2-D inversion

modeling confirmed dominance of solute diffusion, but clearly identified macropore heterogeneity that increased advection transport; 3-D inversion modeling proved relatively ineffective. This study demonstrates the effectiveness of electrical resistivity characterization for delineating heterogenic and anisotropic controls on solute migration that are often poorly defined in simple numerical modeling.

INTRODUCTION

The Carrizo-Wilcox Aquifer is one of the largest aquifers in the State of Texas, supplying over 55,000 hectare-meters (445,892 acre-feet) of water per year (TWDB 2003) for as many as 60 counties throughout eastern portions of Texas. Due to economic significance, the Carrizo-Wilcox Aquifer continues to be investigated for rates of recharge/discharge and solute transport through well monitoring and numerical modeling. Although this aquifer has been the focus of many studies (e.g. Berg 1979; Dutton 2003; Fryer 2003; Mace 2000), the overlying confining beds of the Reklaw Formation have been hydrogeologically neglected in research. The Reklaw is dominated by glauconitic shales that inhibit recharge in areas where Carrizo and Wilcox formations do not crop out, and thus is assumed to be a hydraulic barrier for potential contaminant introduction into the underlying aquifer. The vertical hydraulic conductivity of the Reklaw is primarily controlled by near-continuous marine muds and shales within the formation (Fryar et al. 2003).

Although traditional methods of determining hydraulic conductivity and transmissivity of a formation are considered reliable, additional modeling and analyses can increase accuracy. By implementing electrical resistivity methods, along with numerical modeling, the low hydraulic conductivity and potential solute transport

mechanisms can be better characterized. Both 2-D and 3-D electrical resistivity surveys can be helpful in identifying lithologic variations in resistivity, assist in determining the difference in saturated and unsaturated media, and track solute plumes (Aizebeokhai 2002; Cardimona 2002; Loke 2015). Because certain dissolved solids result in higher or lower resistivity measurements, a plume incorporated with elevated dissolved solids to reduce contact resistance can be tracked more easily over time, as it migrates through the vadose and phreatic zones. In this study, infiltration of an aqueous salt solution was used as a marker for electrical resistivity data collection to differentiate stratum heterogeneity and anisotropy through delineation of variance in electrical conductivity, compared to non-saline saturated and unsaturated host media. The saline solution introduced into the subsurface consisted of 35 g/L (35 ppt), with a total amount of five liters (1.32 gallons) of solution being administered at the beginning of this study.

This study was conducted in central Nacogdoches County within a forested watershed composed of mixed hardwoods (Figure 1). The marine shales studied in this project are part of the Reklaw Formation that crops out throughout the northeastern portions of Texas as an upper, semi-confining, hydrostratigraphic boundary of the Carrizo-Wilcox Aquifer. The Reklaw Formation is part of the Claiborne Group, which are Middle Eocene sedimentary strata that exhibit interfingering of marine and non-marine sediments (Berg 1979). These glauconitic shales are common in East Texas environments and suitable for temporal electrical resistivity modeling of solute

migration due to their natural, relatively low contact resistance; solute plume migration through single event infiltration within low permeability Reklaw strata was monitored for five months using 2-D and 3-D electrical resistivity surveying methods.

Although this study involved five months of data collection in 15 day intervals, data from days 15, 45, 75, 105 and 135 after solute introduction are presented here for discussion of groundwater flow behavior, solute plume delineation and coupled numerical modeling.

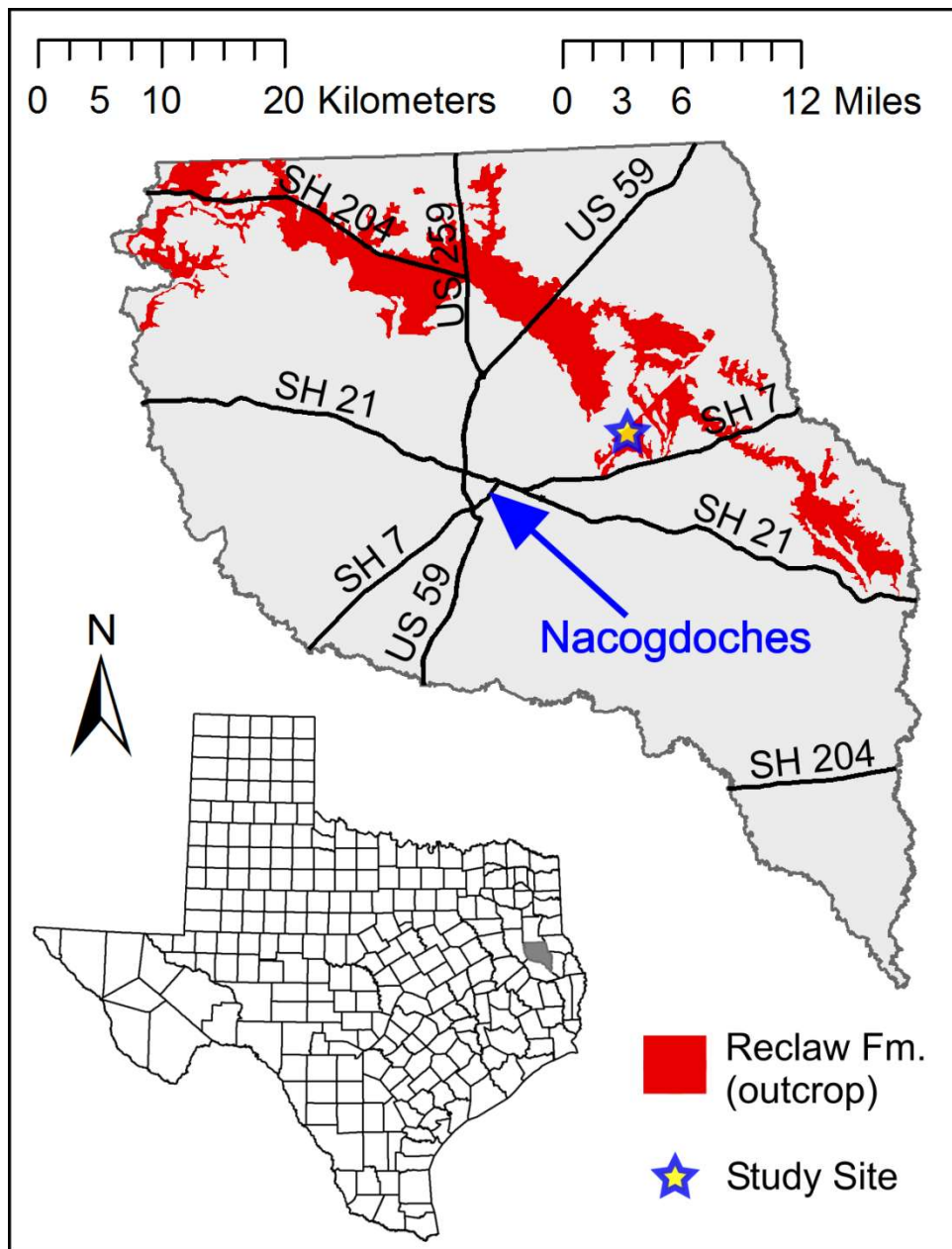


Figure 1. Location of the study area within the Reclaw Formation in Nacogdoches County, Texas. Outcrop area of Reclaw Formation is shown in red; study site is represented by the star east of Nacogdoches, Texas.

STUDY AREA

The Gulf Coastal Plain of East Texas is primarily composed of Paleocene to Eocene marine and non-marine sedimentary rocks. During the early Mesozoic, Pangea began disassembling, causing extensive deformation that produced a geosyncline suitable for early Gulf of Mexico evaporite deposition. Jurassic evaporite deposition and influx of terrestrial sediments induced subsidence of the Gulf Coast, which continued through the Cretaceous as epicontinental seas extended northward (Ewing et al 1960; Garrison and Martin 1973). During the Paleogene, the gulf coastal zone prograded south to southeast, allowing the accumulation of shallow-marine and nonmarine sediments, which exhibited lobate patterns, interspersed with beach and bar systems (Garrison and Martin 1973; Hosman 1996). The deposition of interfingering marine and non-marine sediments led to the formation of the Claiborne Group, which is represented by three fairly rapid marine transgressions followed by slower regressions (Berg 1970; Eargle 1968).

The Claiborne Group is comprised of the Carrizo Sandstone, Reklaw Formation, Queen City Sandstone, Weches Formation, Sparta Sandstone, Cook Mountain Formation, and the Yegua Formation (Figure 2). Carrizo Sandstone is the basal formation of the Claiborne Group, deposited upon the underlying eroded Wilcox Group.

Era	System	Series	Group	Formation
Cenozoic	Paleocene	Eocene	Claiborne	Yegua
				Cook Mountain
				Sparta
				Weches
				Queen City
				Reklaw
				Carrizo
			Wilcox	Upper Wilcox
				Middle Wilcox
				Lower Wilcox

Figure 2. Stratigraphic column of the Claiborne Group. Aquifer bearing horizons highlighted in blue (modified from Watkins, 2018; Fisher, 1964; Forestar, 2011).

The Carrizo was deposited during a marine regression and shows regressive succession of barrier island deposits from beach and shoreface sediments through dune and lagoonal environments (Berg 1979). Reklaw strata conformably overlies the Carrizo Sandstone throughout portions of East Texas; the loamy nature of Reklaw indicates shallow water deposition, just beyond the zone of wave action (Wendlandt and Knebel 1929). The lowermost Reklaw contains brown glauconitic clays and dark-blue, micaceous, sandy clays, with zones of hematite-cemented ironstone concretions (Wendlandt and Knebel 1929). The uppermost Reklaw consists of dark grey to brown, fossiliferous lignitic, and laminated clays (Berg 1979). Queen City Sandstone conformably overlies the Reklaw throughout East Texas. Queen City was deposited along a shallow marine shoreline, as very fine- to medium-grained quartz sand, with interbedded layers of dark carbonaceous shale, silt, and impure lignite (Hosman 1996). In sequential order, the Weches, Sparta, Cook Mountain, and Yegua formations were conformably deposited on top of the Queen City (Berg 1979; Hosman 1996; Stenzel 1938; Wedlandt and Knebel 1929) as proximal coastal deposits associated with minor transgressions/regressions.

The Reklaw Formation is the upper, semi-confining boundary of the Carrizo-Wilcox Aquifer which stretches throughout eastern Texas and into Arkansas and Louisiana. The Carrizo-Wilcox Aquifer is composed of the Hooper, Simsboro, and Calvert Bluff formations of the Wilcox Group and the Carrizo Sand of the Claiborne Group,

which lies unconformably over the Wilcox Group (Mace et al. 2000). This aquifer is bounded below by marine deposits of the Midway Group and above by the Reklaw Formation, which creates a semi-confining horizon between Carrizo Sandstone and the minor aquifer of the Queen City Formation (Fryar et al. 2003). The Reklaw exhibits extremely low permeability, restricting groundwater movement between the Carrizo and the overlying Queen City formations, and acts as a low permeability boundary to reduce potential contaminant migration into the Carrizo-Wilcox Aquifer from shallow subcrop sources. Reklaw permeability is generally reported as exceptionally low with a vertical hydraulic conductivity of approximately $7.9\text{E-}05$ m/day ($2.6\text{E-}04$ ft/day) (Fogg et al. 1983).

Within the Interior Coastal Plain, the study area is dominated by five soil series: Tuscosso, Hannanatchee, Nacogdoches, Sacul, and LaCerde; however, soils at the study site are limited to LaCerde series. LaCerde soils are maturely weathered with low organic and carbonate lime content formed by heavy weathering driven primarily by oxidation of iron-rich minerals (e.g. hematite) that produce red, yellow, or brown iron oxides. Although these soils are highly weathered, they sustain significant vegetation as demonstrated by the mixed deciduous forest of the study site, including several dominant species: mockernut hickory (*Carya tomentosa*), loblolly pine (*Pinus taeda*), white oak (*Quercus alba*), winged elm (*Ulmus alata*), sweetgum (*Liquidambar styraciflua*), white ash (*Fraxinus americana*), southern red oak (*Quercus falcata*), willow

oak (*Quercus phellos*), post oak (*Quercus stellata*), eastern red cedar (*Juniperus virginiana*), and american holly (*Ilex opaca*).

The climate of the region is variable; maximum precipitation typically occurs late fall to early spring with a ten-year historical average of 128.5 cm (50.6 inch) (NOAA 2019). Average annual high temperature is 24.8 °C (76.6 °F), average annual low temperature is 12.4 °C (54.3 °F) and average annual precipitation is 125.1 cm (49.25 inch) (NOAA 2019). During the study period (June 2019 to November 2019), the maximum and minimum temperatures were 34.2° C (93.6 °F) and 5.0 °C (41 °F) in July and October, respectively. Precipitation varied throughout the study period ranging from a low of 0.03 cm (0.01 inch) in August to a high of 0.81 cm (0.32 inch) in November (Figure 3) (NOAA 2019).

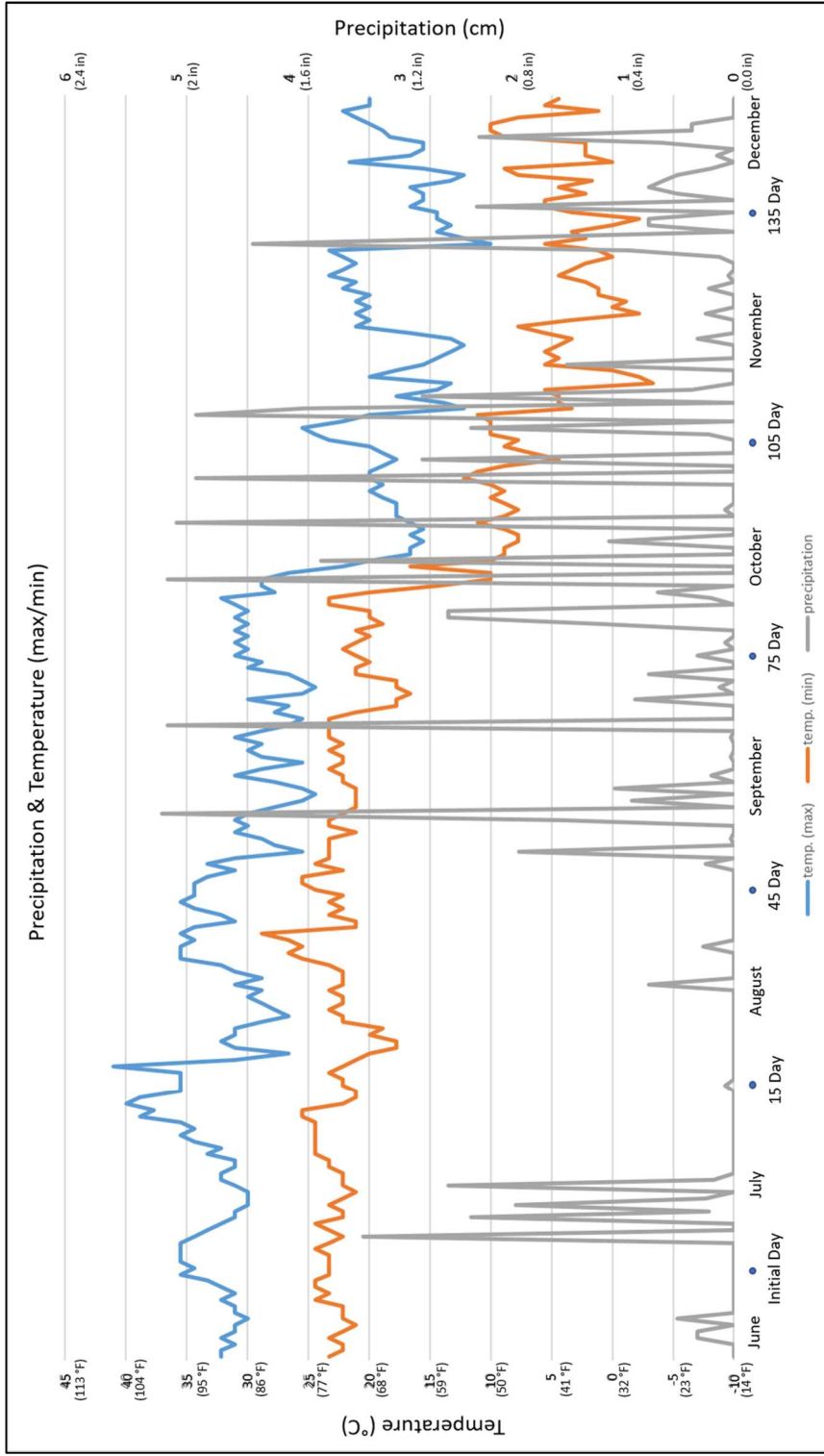


Figure 3. Temperature (maximum and minimum) and precipitation variations within the region of the study area from the month of June to December. Blue dots are indicating the days at which both 3-D and 2-D electrical resistivity measurements were recorded.

ELECTRICAL RESISTIVITY METHODS

Two-dimensional (2-D) and three-dimensional (3-D) direct current (DC) resistivity surveys were conducted over a five-month period within a single 14 by 26 meter (46 X 85 feet) grid. Surveys were conducted using an Advanced Geoscience Inc. (AGI) SuperSting (R8/IP) multi-electrode earth resistivity meter. 2-D electrical resistivity surveys were conducted using dipole-dipole array configuration with one meter (3.3 feet) electrode spacing; 3-D surveys used radial dipole-dipole array configuration with two meter (6.6 feet) electrode spacing to ensure high accuracy and increased shallow depth resolution. Arrays were selected for high sensitivity to horizontal variations, but relatively low sensitivity to vertical variations (Aizebeokhai 2010). Because electrode spacing dictates depth of penetration and profile resolution, small electrode spacing was utilized throughout the survey; as electrode spacing increases, so will depth of penetration, however resolution within the shallower depths will decrease (AGI 2016).

Due to the study area predominantly consists of clay sediments, electrical contact resistance between the ground and each electrode was maintained below 1,500 Ωm (4,900 Ωft). If initial electrode contact resistance exceeded 1,500 Ωm

(4,900 Ω ft), then electrodes were wetted with non-saline water prior to the survey to lower contact resistance below 1,500 Ω m (4,900 Ω ft). Both 2-D and 3-D electrical resistivity surveys were conducted using time estimates of 800 ms and cycled twice per electrode pair. The SuperSting (R8/IP) was set to inject a 2,000 mA current for each survey measurement and was set to reach a maximum error threshold of 2% between measurement cycles.

Recorded resistivity measurements were processed with AGI Earthimager 2-D/3-D inversion modeling software. Both 2-D and 3-D pseudosections were inverted with default surface setting, using smoothing model inversion; max RMS error and error reduction percentages were unselected, while smoothness factor and damping factor were set to 10. To improve inverted resistivity models, data outliers, less than 10%, were removed using data misfit histograms. Terrain correction was incorporated into resistivity sections to better constrain the relationship between topography and electrical resistivity analyses; terrain files were constructed through hydro-leveling at the study site with sub-centimeter (<0.5 in) accuracy.

NUMERICAL MODELING METHODS

Following 2-D and 3-D electrical resistivity analyses, numerical modeling was conducted to independently evaluate hydraulic conductivity and solute transport within Reklaw strata. Within the 14 by 26 meter (46 X 85 feet) survey grid, infiltration tests, piezometer slug tests, and sediment analyses were conducted to aid in the development of numerical models. Infiltration tests were conducted in four different locations using Turf-Tec infiltration rings with four iterations per infiltration site; all infiltration ring sites were within four meters (13 feet) of solute introduction location (Figure 4). Although none of the soil infiltration tests reached steady state infiltration, they did approach these conditions.

Slug tests were conducted on three, previously installed piezometers within the study area; slug test data were acquired using Solinst Leveloggers pressure transducers with initial piezometer head measured using a Solinst Mini Water Level Meter Model 102M. Slugs of 500 ml (30 in³), 1000 ml (60 in³) and 2000 ml (120 in³) were introduced into each piezometer and allowed to equilibrate for a minimum of six hours. All slug tests were repeated a minimum of three times and average hydraulic conductivity was calculated for each well using the Hvorslev method (Hvorslev 1951).

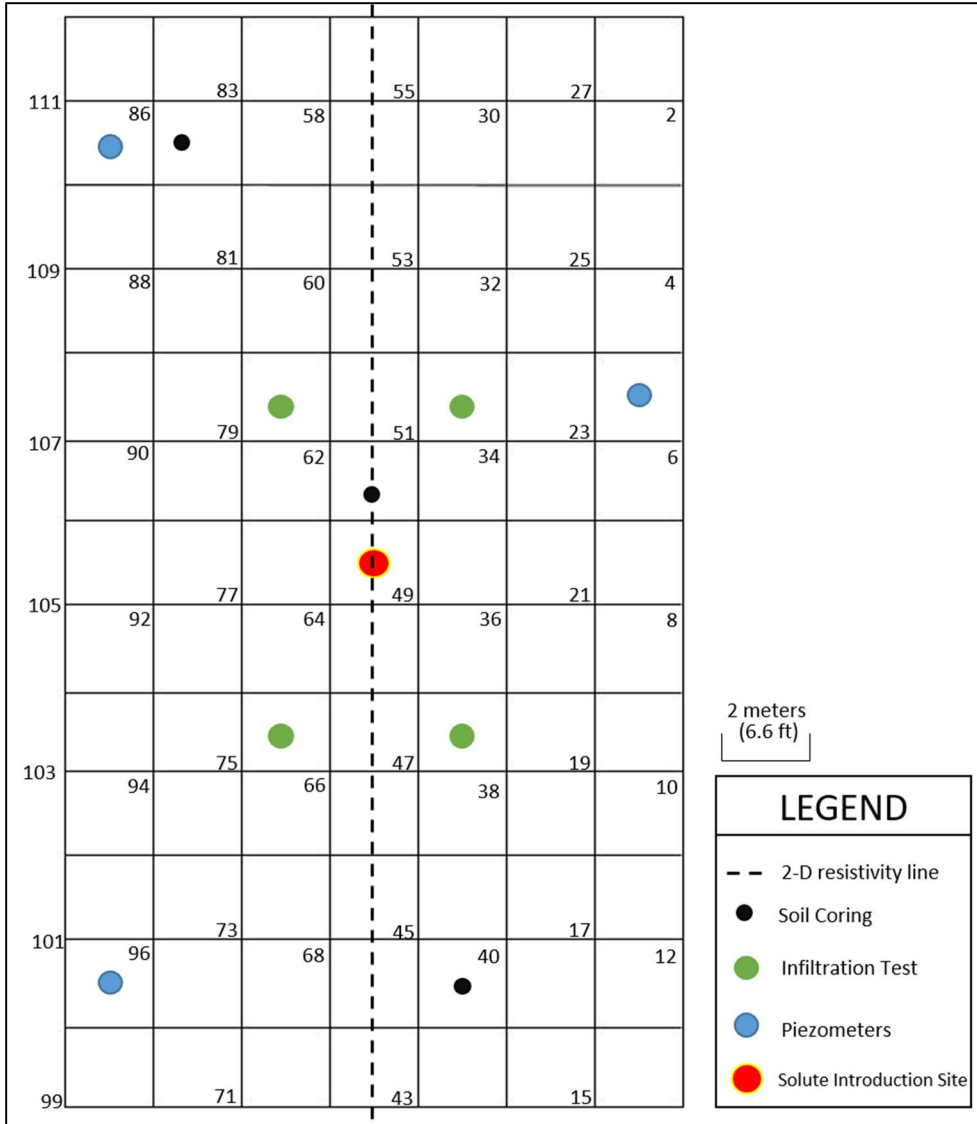


Figure 4. Plan view of the study site showing location of each piezometer, soil coring, and infiltration test conducted, as well as the location for every other electrode labeled within the 3-D resistivity array.

Sediment analyses were conducted using cores collected from three locations within the study area; each core was 250 cm (98 inch) deep and sampled in 10 cm (4 inch) increments (n=75). Bulk density was calculated based on methods described by Fetter (2001), which averaged 1.68 g/cm³ (105 lb/ft³). Hydraulic conductivity based on particle size distribution was calculated using the methods presented by Svensson (2014). Effective porosity was calculated for each interval based on the methods presented by Stephens et al. (1998); bulk density and particle size analyses for each sample increment were calculated; particle size analyses were conducted using the hydrometer method (Bouyoucos 1962). Bulk density analyses were conducted to determine volumetric water content and porosity; porosity was calculated based on average particle density of 2.65 g/cm³ (165 lb/ft³) for siliciclastic sediments (Fetter 2001) and measured bulk density. Particle size analyses were used to determine vertical anisotropy in porosity and hydraulic conductivity in order to develop solute transport modeling of advection, hydrodynamic dispersion, adsorption, and retardation.

Advection, driven by hydraulic gradient, is usually the predominant process for solute transport (Postigo et al. 2018). Solute transport is a function of the flow rate and solute concentration within groundwater (Fetter 2001), where solute advection is a function of average linear velocity. Average linear velocity was calculated as:

$$v_x = \frac{K}{n_e} \frac{dh}{dl} \quad (1)$$

where, v_x is average linear velocity, K is hydraulic conductivity, n_e is effective porosity, and dh/dl is the hydraulic gradient.

Hydrodynamic dispersion includes molecular diffusion and mechanical dispersion (Fetter 2001), where solutes being transported through dispersion are a function of flow pattern heterogeneity within sediment. Solute dispersion results in both longitudinal and transverse flow migration represented by equations from Fetter (2001):

$$\begin{aligned}D_L &= \alpha_L v_i + D^* \\D_T &= \alpha_T v_i + D^*\end{aligned}\tag{2}$$

where, D_L is hydrodynamic dispersion coefficient parallel to the principle direction of flow (longitudinal), D_T is hydrodynamic dispersion coefficient perpendicular to the principle direction of flow (transverse), α_L is longitudinal dynamic dispersivity, α_T is transverse dynamic dispersivity, and D^* is the effective diffusion coefficient.

Adsorption and retardation are similar processes that hinder the rate at which solute migrates. Adsorption occurs in porous materials when solutes diffuse and adhere (sorbed) to the surface of grain particles, thus reducing or retarding solute transport (Wood et al. 1990). Adsorption for the study site was calculated as a linear sorption isotherm as described by Travis and Etnier (1981):

$$C^* = K_d C\tag{3}$$

where, C^* is the mass of solute sorbed per dry unit of weight of solid, C is the concentration of solute in solution in equilibrium with the mass of solute sorbed on the

solid, and K_d being the distribution coefficient. The distribution coefficient (K_d) for chlorine (Cl) was modeled at 1.7E-3 for clay sediments as reported by Sheppard et al. (2009). Using their distribution coefficient, the retardation factor was calculated using the equations of Anderson (1979), Faust and Mercer (1980), Prickett et al. (1981), and Srinivasan and Mercer (1988):

$$1 + \frac{B_d}{\vartheta} K_d = r_f \quad (4)$$

where, r_f is the retardation factor, B_d is bulk density of the soil and ϑ is the porosity of saturated media. These data for advection, dispersion, adsorption and retardation were used to model the spatial pattern of solute plume development in one-dimensional and two-dimensional uniform flow fields. Calculation of solute concentration in a one-dimensional field was evaluated based on the equation by Crank (1956):

$$C_i(x, t) = C_0 \operatorname{erfc} \frac{x}{2(D^*t)^{0.5}} \quad (5)$$

where, C_i is the solute concentration at distance x from the source at time t since solute introduction, C_0 is the original concentration, which remains a constant, and erfc is a complementary error function (Fetter 2001). Calculation of concentration of the solute plume within a two-dimensional field followed the method of De Josselin and De Jong (1958):

$$C(x, y, t) = \frac{C_0 A}{4\pi t (D_L D_T)^{0.5}} \exp \left[-\frac{((x-x_0)-v_x t)^2}{4D_L t} - \frac{(y-y_0)^2}{4D_T t} \right] \quad (6)$$

where, A is the area in square centimeters. The concentrations at a distance x, y and time t were grid formatted and imported into Surfer software for graphical model generation. Numerical modeling of solute plumes were calculated for 15, 45, 75, 105, and 135 days after the solute introduction to compare with resistivity analyses in this manuscript.

RESULTS AND DISCUSSION

Throughout this study, various techniques were employed to evaluate solute plume migration patterns within the Reklaw Formation. Slug tests were conducted on three piezometers within the study area (Figure 4) to determine the hydraulic conductivity using the Hvorslev method (Fetter 2001); piezometers 1, 2 and 3 exhibited hydraulic conductivities of $7.15\text{E-}06$ cm/sec ($2.8\text{E-}06$ in/sec), $2.02\text{E-}04$ cm/sec ($7.95\text{E-}05$ in/sec) and $1.86\text{E-}04$ cm/sec ($7.32\text{E-}05$ in/sec), respectively. Temporal water table variations within the study site were monitored from June to November, indicated total water table fluctuations of less than one meter (three feet) throughout the study duration and less than ten centimeters (four inches) within any diurnal cycle.

Soil borings were conducted at three locations within the study site to assess local heterogeneity and anisotropy. Borings were collected in 10 cm (4 inch) increments to a depth of 250 cm (98 inch) to determine bulk density and particle size composition in order to calculate variability in hydraulic conductivity (Figure 5). Hydraulic conductivity based on core analyses ranged from $1.05\text{E-}02$ cm/sec ($4.1\text{E-}03$ in/sec) to $1.67\text{E-}05$ cm/sec ($6.5\text{E-}06$ in/sec), but averaged $4.14\text{E-}03$ cm/sec ($1.6\text{E-}03$ in/sec). Surface infiltration ranged from $2.0\text{E-}03$ cm/sec ($7.8\text{E-}04$ in/sec) to $2.0\text{E-}02$ cm/sec ($7.8\text{E-}03$

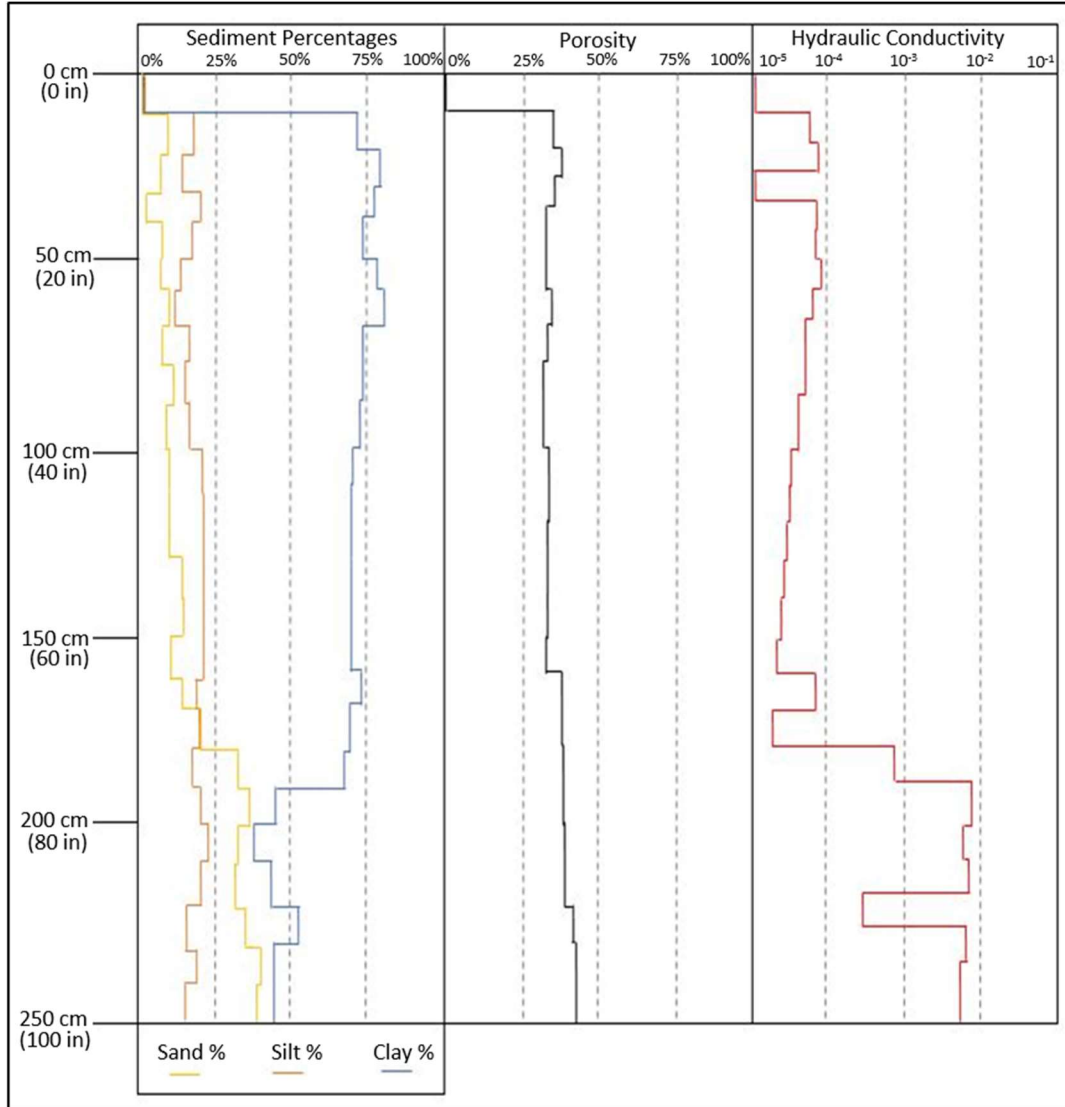


Figure 5. Particle-size distribution, porosity, and hydraulic conductivity values from ground level to 250 cm (98 in) deep for sediment core sampling proximal to solute introduction location. Hydraulic conductivity values in graph are measured in cm/sec.

in/sec) based on standard infiltration ring analyses within the study area, confirming that calculated hydraulic conductivities were reasonable.

2-D and 3-D electrical resistivity methods were employed to map solute plume migration in 15-day intervals following solute injection. The introduced solute consisted of five liters (300 in³) of 35 g/L (35 ppt) NaCl that was inserted between electrodes 49, 50, 64, and 65 of the 3-D study grid (Figure 4) or between electrodes 13 and 14 in the 2-D survey line; solute introduction was via a plastic liner installed 20 cm (8 in) into the land surface with a diameter of 30 cm (12 in) and a perforated bottom. The 3-D resistivity survey grid was the primary reference used to model solute plume movement over the five month duration of this study.

3-D RESISTIVITY ANALYSES

All 3-D surveys were conducted with 112 electrodes in the same location and a survey grid oriented in NW-SE trending lines, with 14 electrodes along the y-axis and 8 electrodes along the x-axis in uniform two meter (6.6 feet) spacing to produce a survey grid with a depth resolution of approximately 6.5 meters (21 feet) (Figure 6).

Background resistivity data were collected prior to the five-liter (300 in³) solute solution introduced on June 28, 2018.

3-D: Initial Conditions

The initial 3-D survey was conducted prior to solute plume infiltration, core sampling, and infiltration ring analyses, in order to acquire minimally-disturbed background data of the study site (Figure 6A). Initial 3-D survey data exhibit significant variance in resistivity measurement throughout the survey and unsaturated conditions extended to more than 2.5 m (8.2 feet) deep up gradient and less than 1.5 m (4.9 feet) deep down gradient. Minor variations in resistivity at shallow depths are attributable to root structures and associated vegetation within the forested watershed. Resistivity variations at depth are attributed to heterogeneous iron cements throughout the Reklaw Formation. This initial model suggests relatively simple, layered strata with anisotropy and heterogeneity induced by a combination of biotic and abiotic anomalies.

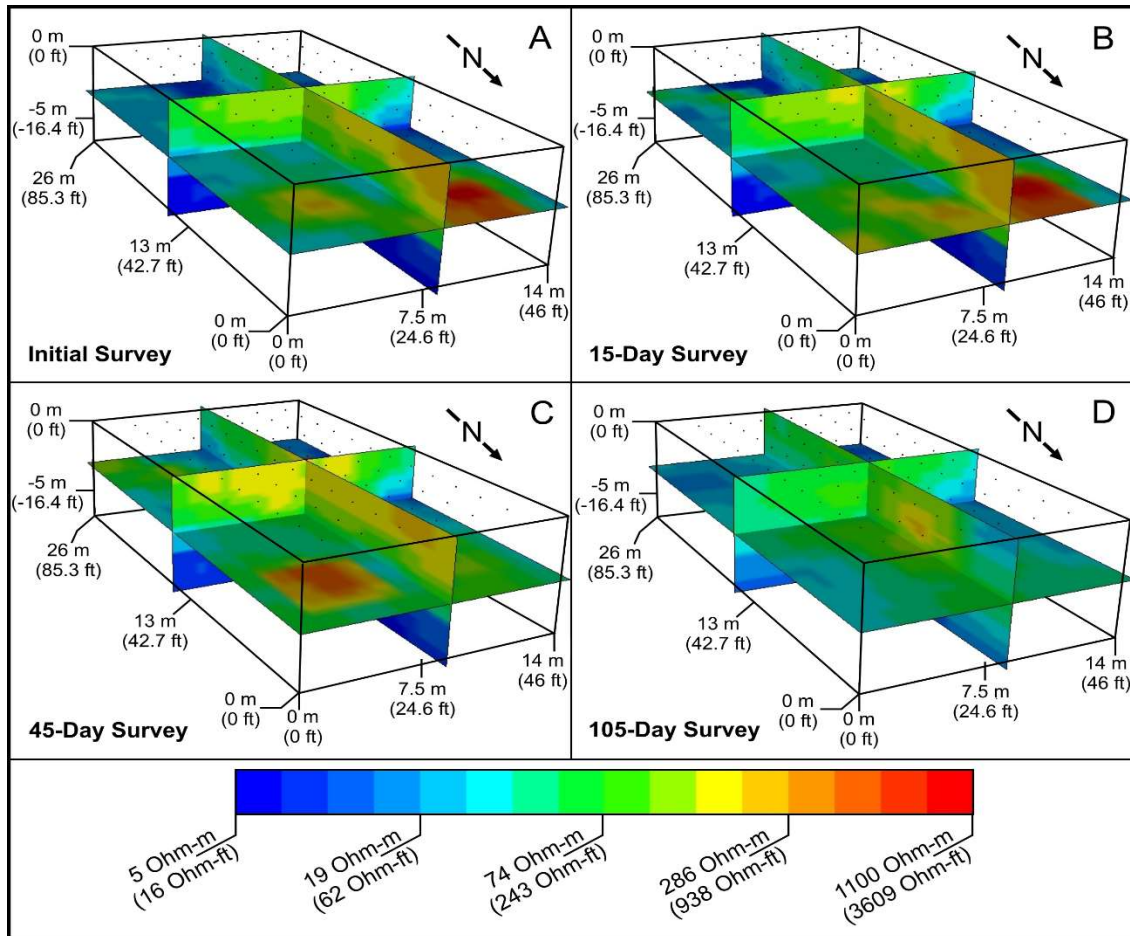


Figure 6. Dynamic slices of 3-D inverted resistivity models: A) Initial background survey (Day 1) (RMS = 8.8%, L2 norm = 1.1, iteration = 8); B) 15-day survey (RMS = 6.9%, L2 norm = 1.0, iteration = 8); C) 45-day survey (RMS = 2.8%, L2 norm = 0.2, iteration = 8); D) 105-day survey (RMS = 2.2%, L2 norm = 0.8, iteration = 8).

3-D: 15-Day Survey

The 15-Day Survey following solute infiltration showed similar conditions to background 3-D resistivity survey analyses, with a slight decline in the interpreted water table depths of approximately 50 cm (20 in), based on variation of high and low resistivity measurements (Figure 6B). Heterogeneities in the upper portion are more distinct and are associated with declining water table effects on local vegetation, while anomalies in the lower portion remain relatively consistent. The solute infiltration site in the center of the survey grid did not produce any visible anomaly; however, a minor decrease in resistivity is observed at a depth of approximately 75 cm (30 in), seen in the small elliptical resistivity anomaly near the upper convergence of the two vertical slices in the figure 6B. This minor anomaly is likely the result of solute infiltration; however, variation in resistivity at this location is not significant compared to other anomalies within the 3-D resistivity survey and would likely not be discernable if this was not an experimental project with known solute infiltration data.

3-D: 45-Day Survey

The 45-Day Survey continued to demonstrate similar conditions to the initial background 3-D survey but experienced a greater decrease in the water table to approximately 60 cm (24 in), indicated by the high resistivity values during this survey (Figure 6C). This decrease in soil moisture can be attributed to the increased moisture absorption from the surrounding vegetation, due to a lack of precipitation during the

month of July. After 45 days of solute plume migration, an area located within the center of the survey grid demonstrated an area of lower resistivity at a depth of approximately 85 cm (33 in), which was perceived to be the solute plume; however, due to a variety of irregular anomalies produced by the AGI software, this could not be definitively proven; 75-Day 3-D resistivity survey data did not appear significantly different than 45-Day resistivity survey data and thus was excluded from this manuscript.

3-D: 105-Day Survey

The 105-Day Survey indicates higher moisture content throughout the survey grid with subdued geophysical anomalies (Figure 6D). Saturated conditions do not appear to have risen significantly within the study site as compared to the 15-Day Survey; however, total soil moisture appears to have increased as a result of multiple precipitation events from June to November of 2018. Reduction in anomalies in the upper zones is likely attributable to a decrease in evapotranspiration during late fall with the seasonal shift in water uptake by trees in the study area within this forested watershed. As with the 15-Day Survey, a slight decrease in resistivity appears in the 105-Day resistivity inversion at the site of solute infiltration (Figure 6D) and extends from the surface to more than a meter (three feet) deep and nearly two meters (seven feet) in diameter. Because it is improbable that solute migration would have occurred

significantly upward towards the land surface, this anomalous rise is attributed to increased local recharge due to initial soil disturbance at the site of solute infiltration.

2-D ANALYSES AND NUMERICAL MODELING

2-D resistivity surveys were conducted with 28 electrodes at one-meter-spacing (3.3 feet) in the same location and orientated in an NW-SE trending line through the center of the 3-D survey grid, producing 27-meter-long (89 feet) survey lines with depth resolution of approximately three meters (ten feet). Complimentary numerical modeling was conducted based on field-derived calculations of hydraulic conductivity in order to assess predictive modeling of solute migration as compared to geophysical monitoring through resistivity analyses.

2-D: 15-Day Analyses

Numerical modeling and 2-D resistivity analyses conducted 15 days after the solute was introduced (Figure 7A & 8A) indicate low saturated surface material to a depth of approximately one meter (3.3 feet); the top of the water table at 15 days was 1.6 m (5.2 ft) deep. Between electrodes 13 and 15, resistivity analyses showed the solute plume (Figure 7A) was 75 cm (29.5 inch) wide and extended to a depth of one meter (3.3 feet). Refined resistivity inversion conducted between electrodes 9 and 18 (Figure 8A) indicated more complex migration behavior with a solute plume 50 cm (20 in) wide that descended near-vertically for 40 cm (16 in), migrated predominantly laterally to the southeast for 50 cm (20 in), and then again migrated near vertically for an additional 40 cm (16 in).

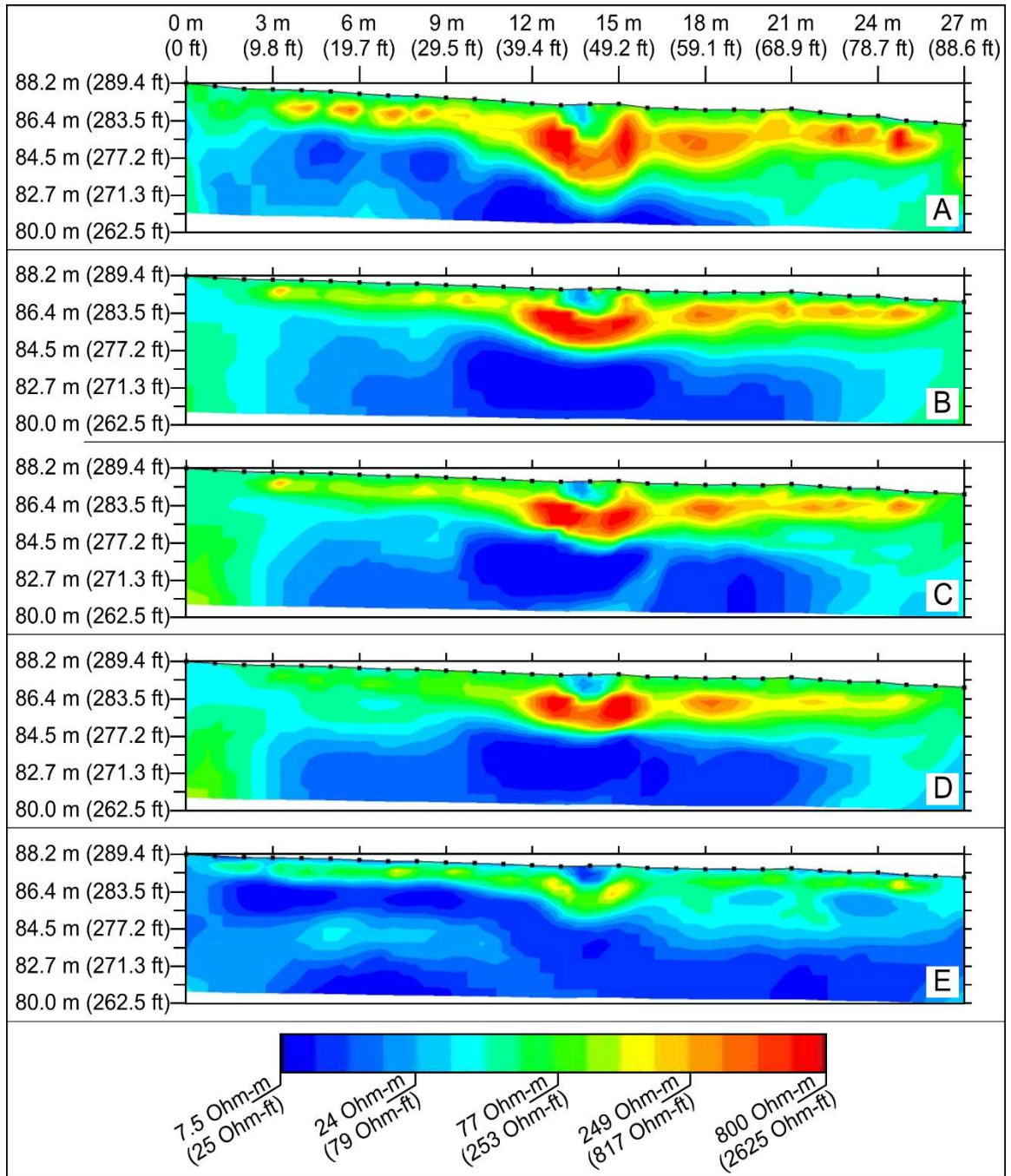


Figure 7. 2-D inverted electrical resistivity sections: A) 15-day survey (RMS error = 2.57%, L2 norm = 0.73, iteration = 8); B) 45-day survey (RMS error = 2.44%, L2 norm = 0.65, iteration = 8); C) 75-day survey (RMS = 2.91%, L2 norm = 0.93, iteration = 8); D) 105-day survey (RMS = 2.24%, L2 norm = 0.55, iteration = 8); E) 135-day survey (RMS = 3.66%, L2 norm = 1.22, iteration = 8).

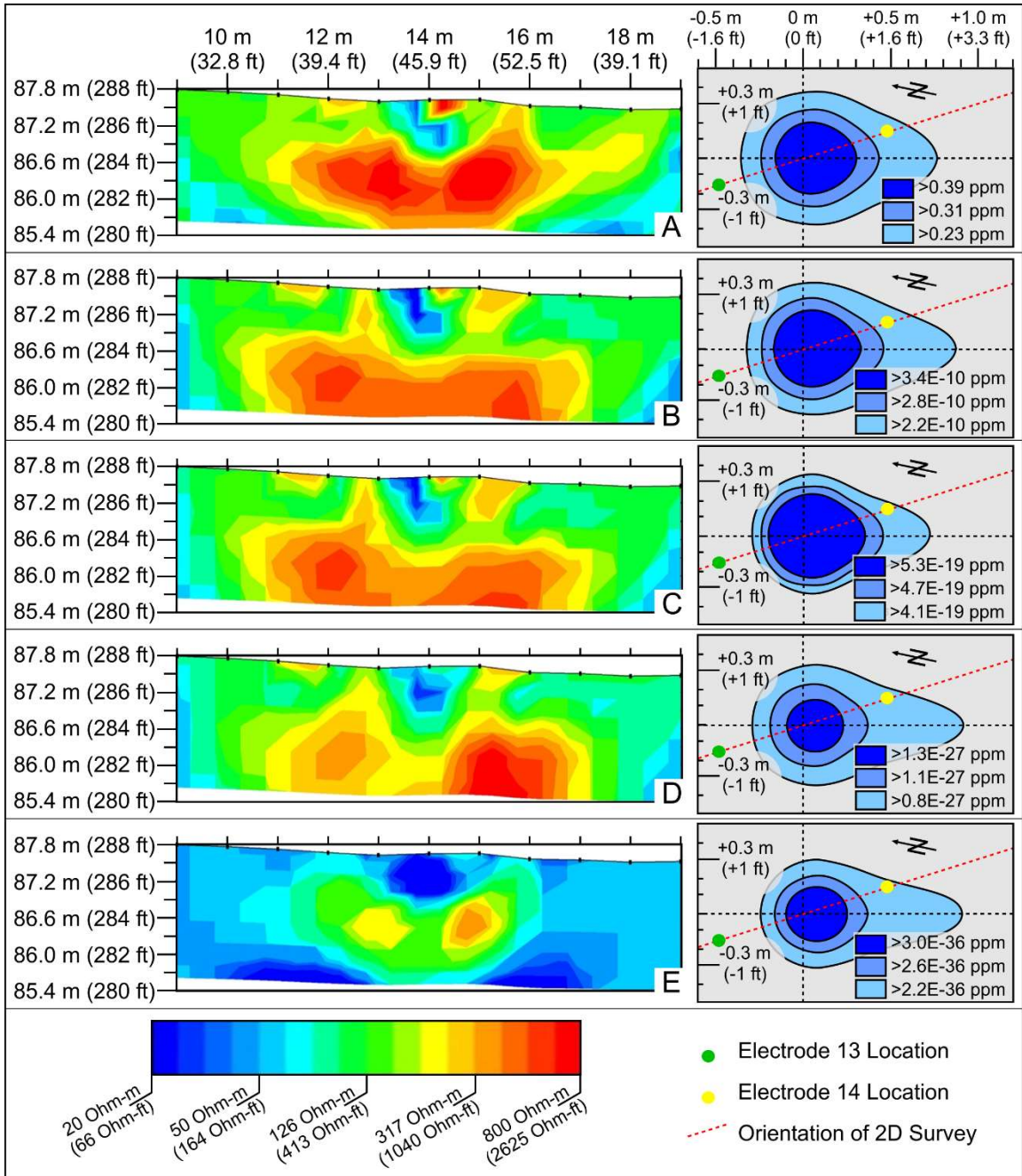


Figure 8. Refined inverted resistivity sections (left) with associated numerical model (right): A) 15-day survey (RMS error = 1.46%, L2 norm = 0.24, Iteration = 8.); B) 45-day survey (RMS error = 2.09%, L2 norm = 0.48, Iteration = 8.); C) 75-day Survey (RMS error = 1.98%, L2 norm = 0.36, Iteration = 8.); D) 105-day survey (RMS error = 1.82%, L2 norm = 0.37, Iteration = 8.); E) 135-day survey (RMS error = 1.79%, L2 norm = 0.32, Iteration = 8).

Numerical solute modeling (Figure 8A) suggested that the center (highest concentration) of the solute concentration plume migrated 10 cm (4 in) in the direction of advection (water table mapping indicates advection within the study site is oriented at 192 degrees azimuth) with the bulk of the solute migration induced by diffusion (modeling indicates that most solute concentration was <0.5 mg/L (<0.5 ppm) after 15 days). Comparison of 2-D numerical modeling in horizontal, homogeneous and isotropic media underestimated the extent of solute migration at 15 days as compared to the more complex solute migration patterns documented in 2-D vertical resistivity profiling. While the solute plume did not move significantly based on resistivity analyses, geophysical data illustrated well the complexity of vertical heterogeneity within the Reklaw Formation where permeability boundaries promoted lateral movement interspersed with vertical solute migration most likely along macropores. Various locations of higher resistivity were observed throughout the upper portion of the study site, due to the abundance of unsaturated material and vegetation variability within forested watersheds.

2-D: 45-Day Analyses

Numerical modeling and 2-D resistivity analysis conducted 45 days after solute injection (Figure 7B & 8B) continued to demonstrate low saturated media to a depth of approximately two meters (6.6 ft); the top of the water table at 45 days was 2.3 m (7.5 ft) deep. Between electrodes 13 and 15, the size of the solute plume (Figure 7B)

increased to 80 cm (32 in) wide and remained 100 cm (3.3 ft) deep. Refined resistivity inversion between electrodes 9 and 18 (Figure 8B) indicated the solute plume was 70 cm (28 in) wide that descended nearly vertically for 60 cm (24 in), before it migrated laterally to the southeast for 50 cm (20 in).

The 45-Day spatial pattern of solute transport was similar to the 15-Day analyses but showed greater lateral migration both down- and up-gradient from initial solute introduction, suggesting greater solute diffusion effects. According to numerical solute modeling (Figure 8B), the center of the solute concentration plume should have been located 12 cm (4.7 in) in the direction of advection with the majority of the solute migration prompted by diffusion. Solute modeling after 45 days indicated the concentration had decreased to $<6E-10$ mg/L (ppm). 2-D vertical resistivity images continued to indicate areas of high resistivity among the upper portions of the study site due to unsaturated material, increased porosity and vegetation.

2-D: 75-Day Analyses

Numerical modeling and 2-D resistivity analysis conducted 75 days after solute injection (Figure 7C & 8C) show an increase in low saturated media, reaching a depth approximately 2.3 m (7.5 ft); the top of the water table at 75 days was approximately 3.1 m (10 ft) deep. Resistivity analyses between electrode 13 and 15 (Figure 7C) indicate the solute plume increased to 85 cm (34 in) wide, but remained vertically stagnant, retaining a depth of 100 cm (3.3 ft). Refined resistivity inversion between electrode 9

and 18 (Figure 8C) indicated a solute plume 70 cm (28 in) wide that descended nearly vertically for 60 cm (24 in), before migrating laterally to the southeast for 40 to 45 cm (16-18 in). Numerical solute modeling (Figure 8C) suggested the center of the solute plume should not have shifted laterally nor transversely since the 45-day interval; however, solute modeling after 75 days indicated the concentration decreased to $< 9\text{E-}19$ mg/L (ppm). Two-dimensional resistivity inversion images continued to locate areas of low saturated material and vegetation anomalies, demonstrated by the areas of high resistivity throughout the upper portions of the study site.

2-D: 105-Day Analyses

Numerical modeling and 2-D resistivity analysis conducted 105 days after injection (Figure 7D & 8D) indicated an increase in low saturated media to a depth of approximately 2.8 m (9.2 ft); the top of the water table at 105 days was 3.3 m (11 ft) deep. Resistivity analyses between electrode 13 and 15 (Figure 8D) indicated the solute plume increased to 125 cm (4 ft) wide and reached a depth of one meter (3.3 ft). Refined resistivity inversion between electrode 9 and 18 (Figure 8D) indicated the solute plume of 90 cm (35 in) wide moved laterally 80 cm (32 in), before showing signs of vertical ascension. Numerical solute modeling (Figure 8D) indicated the center of concentration within the solute plume should not have shifted laterally or transversely since 75-day analyses. Solute modeling after 105 days demonstrated a decrease in concentration to $< 3\text{E-}27$ mg/L (ppm). The 2-D resistivity images continued to

demonstrate areas of high resistivity, due to regions of low saturated material and vegetation.

2-D: 135-Day Analyses

Numerical modeling and 2-D resistivity analysis conducted 135 days after injection (Figure 7E & 8E) demonstrated a significant increase in saturated media and water table depth; the top of the water table at 135 days was approximately 90 cm (35 in) deep. Resistivity analyses between electrode 13 and 15 (Figure 7E) indicated the solute plume had increased to 175 cm (5.6 ft) wide and continued to resist vertical subsidence, with a solute plume depth of one meter (3.3 ft). Refined resistivity inversion between electrode 9 and 18 (Figure 8E) indicated the solute plume increased to 100 cm (3.3 ft) wide and moved laterally 90 cm (35 in) since the 105 day model. Numerical solute modeling (Figure 8E) showed the center of concentration should not have migrated further southeast since the 105-day interval, but concentrations should have decreased to $<5E-36$ mg/L (ppm). Due to the high water table depth and increase in saturated media, the areas of low saturation diminished and demonstrated lower resistivity values than previous months.

CONCLUSIONS

Electrical resistivity methods and numerical modeling were used to evaluate solute plume migration over a period of 135 days in strata of the Reklaw Formation. These analyses were developed to evaluate the effectiveness of resistivity methods in characterization of groundwater contaminant migration within low permeability media and forested watersheds; numerical modeling was introduced to compare traditional groundwater modeling methods with site specific geophysical data. Modeled data confirm that the low volume of salt solution introduced in this study would not have had a significant effect on permeability due to potential induced soil swelling because modeled concentrations above ambient conditions are well below 1 mg/L (ppm) in less than 15 days after solute introduction. 3-D resistivity analyses conducted prior to solute introduction allowed for unaltered background data to be compared with changes after the solute was infiltrated.

Data collected from piezometer slug tests represented similar hydraulic conductivity values as compared with infiltration ring tests and particle size analyses, assisting in validation of these results. Hydraulic conductivity values produced through the combination of these tests demonstrated an average of $4.14\text{E-}03$ cm/sec ($1.6\text{E-}03$ in/sec) throughout study site sediments with a minimum and maximum of $1.67\text{E-}05$

cm/sec (6.57E-06 in/sec) and 1.05E-02 cm/sec (4.13E-03 in/sec), respectively. Variability is attributed to heterogeneity and anisotropy throughout the Reklaw Formation.

Resistivity analyses were conducted using an AGI SuperSting (R8/IP) to produce 2-D and 3-D surveys at regular intervals following the introduction of a NaCl solute solution into the groundwater system. The NaCl solution was minor, with only five liters (300 in³) of solute at 35 mg/L (ppt), but allowed resistivity analyses to easily locate the solute plume within the subsurface due to the minor conductance increase.

Resistivity data inversion for 3-D analyses produced models with highly irregular subsurface anomaly boundaries, suggesting that processing software was unable to effectively render models for large 3-D resistivity surveys (at the time of this research, no published studies had incorporated 112 electrodes into a single 3-D resistivity survey with an AGI SuperSting (R8/IP)). In an attempt to improve resistivity analyses, various array configurations (e.g., dipole-dipole, radial-dipole, and mixed gradient) were attempted, but modeled inversions remained consistently poor. While distinct solute plume migration was not documented in 3-D resistivity surveys, minor electrical anomalies proximal to the solute infiltration site suggests that resistivity data may capture small 3-D solute plumes, but inversion modeling could not definitively resolve these plumes as a result of either inversion software limitations or electrode spacing. Future studies should consider reducing electrode spacing to one meter (3.3 ft) on 3-D surveys for solute plume delineation in low permeability media.

The combination of 2-D resistivity surveying and numerical modeling better characterized migration patterns and concentration variances of the solute plume as it migrated through low permeable strata. Over the course of 135 days, 2-D electrical resistivity inversions resolved solute plume migration as it moved transversely; inverted resistivity sections indicate vertical movement reached a total of 100 cm (40 in) deep, with 90 cm (35 in) lateral migration. 2-D resistivity sections tracked the solute as diffusion dominated transverse migration through the subsurface and was also able to characterize this movement in the northwest direction. Numerical models demonstrated migration patterns of the solute plume as it was carried through the subsurface under the combined effects of advection, diffusion, and dispersion. Due to the flow direction of subsurface water (azimuth of 192 degrees), the solute showed dominant movement to the southwest; total migration of the concentration center was approximately 12 cm (4.7 inch) from the site where the solution was introduced, which compared well with the center of concentration documented in resistivity surveys. Combined dispersion and diffusion, over the course of 135 days, caused radial solute plume migration with minor dominance in the direction of advection; effects of diffusion and dispersion are apparent through the decrease in solute concentration from the initial concentration of 35 g/L (ppt) to $<5E-36$ mg/L (ppm) over the time of the study.

Reklaw strata and associated soil within the study site are heterogeneous and anisotropic as evidenced by infiltration ring tests, slug tests, and particle-size analyses.

Due to these conditions, electrical resistivity methods were better equipped than numerical modeling to track solute plume migration patterns because simple numerical modeling assumed homogeneous, isotropic conditions. Additionally, variability in precipitation throughout the study was not incorporated into numerical modeling, which resulted in underestimation of solute migration over the course of 135 days, as numerical modeling assumed steady state conditions.

Electrical resistivity analyses proved more valuable in tracking solute migration patterns through low permeability media, especially 2-D resistivity analyses—3-D inverted resistivity sections poorly delineated the solute plume within the study grid. Because of the effectiveness of 2-D resistivity models, radial 2.5-D resistivity analyses should be incorporated into future solute migration studies in low permeability media to better evaluate 3-D migration patterns. Additionally, more complex numerical modeling should be considered in future studies to account for greater heterogeneity and temporal changes in precipitation.

This study has demonstrated that the Reklaw Formation is highly impermeable with low hydraulic conductivity values, which allows for significant isolation of potential near-surface contaminants to be introduced through semi-confining strata into the underlying Carrizo-Wilcox Aquifer. Data collected during this study clearly demonstrate the effectiveness of electrical resistivity imaging on solute migration delineation and the effectiveness of the Reklaw Formation as a low permeability boundary. Data suggests that

lateral and vertical solute transport in the Reklaw Formation is primarily along macropore structures, but solute transport is dominated by diffusion. The Reklaw appears to be an effective upper boundary for reduction of potential solute transport into the Carrizo-Wilcox Aquifer.

REFERENCES

- AGI. 2016. Seminar on resistivity imaging: AGI Resistivity Imaging Seminar, Sept. p: 7-9.
- Aizebeokhai AP. 2010. 2D and 3D Geoelectrical Resistivity Imaging: Theory and Field Design. 5(23), pp. 3592–3605.
- Anderson, M. P. 1979. Using models to simulate the movement of contaminants through groundwater flow systems. *CRC Critical Reviews in Environmental Control* 9, no. 2:97-156.
- Berg, Robert R. 1979. Stratigraphy of the Claiborne Group. *Houston Geological Society*, pp. 5–11.
- Bouyoucos, G.J. 1962. Hydrometer method improved for making particle size analysis of soils. *Agron. J.* 54:464-465.
- Crank, J. 1956. *The mathematics of diffusion*. New York: Oxford University Press.
- Cardimona, Steve. 2002. *Electrical Resistivity Techniques for Subsurface Investigation*.
- De Josselin De Jong, G. 1958. Longitudinal and transverse diffusion in granular deposits. *Transactions, American Geophysical Union* 39, no. 1:67.
- Dutton, A. et al. 2003. Groundwater Availability in the Carrizo-Wilcox Aquifer in Central Texas. *Bureau of Economic Geology*, pp. 1–405.
- Eargle, D Hoye. 1968. Nomenclature of Formations of Claiborne Group, Middle Eocene, Coastal Plain of Texas, p 1-34.
- Ewing, J., Antoine, J. W., and Ewing, Maurice. 1960. Geophysical measurements in the western Caribbean Sea and in the Gulf of Mexico: *Jour. Geophys. Research*, v. 65, no. 12, pp. 4087-4126.

- Faust, C. R., and J. W. Mercer. 1980. Ground-water modeling: recent developments. *Ground Water* 18, no. 6:569-77.
- Fetter, C. W., Jr. 2001. *Applied Hydrogeology*. 3d ed. New York: Prentice Hall, Inc. pp. 691.
- Fisher, W.L. 1964. *Sedimentary Patterns in Eocene Cyclic Deposits, Northern Gulf Coast Region*, Bureau of Economic Geology, Austin, Texas.
- Fogg, G.E., S.J. Seni, and C.W. Kreitler. 1983. Three-dimensional ground-water modeling in depositional systems, Wilcox Group, Oakwood salt dome area, east Texas. The University of Texas at Austin, Bureau of Economic Geology, Report of Investigations No. 133, pp. 55.
- Forestar. 2011. Map, East Texas Basin.
http://www.forestargroup.com/assets/minerals/FORE_EastTx.pdf
- Fryar, D., Senger, R., Deeds, N., Pickens, J., and Jones, T. 2003. Groundwater Availability Model for the Northern Carrizo-Wilcox Aquifer: Texas Water Development Board, pp. 1–529.
- Garrison, L.E., and Martin, R.G., Jr. 1973. Geologic structures in the Gulf of Mexico basin: U.S. Geological Survey Professional Paper 773, pp. 85.
- Hosman, R.L. 1996. Regional Stratigraphy and Subsurface Geology of Cenozoic Deposits, Gulf Coastal Plain, South-Central United States. U.S. Geological Survey Professional Paper, pp. 1416-G.
- Hvorslev M.J. 1951. Time Lag and Soil Permeability in Ground-Water Observations. Bull. No.36, Waterways Experiment Station, Corps. Of Engineers, U.S. Army, pp. 50.
- Loke MH. 2015. Tutorial: 2-D and 3-D Electrical Imaging Surveys. pp. 1–187
- Mace, R.E., R.C. Smyth, L. Xu, and J. Liang. 2000. Transmissivity, hydraulic conductivity, and storativity of the Carrizo-Wilcox Aquifer in Texas, The University of Texas at Final

Report, 15-7 January 2003 Austin, Bureau of Economic Geology, Final Report submitted to the Texas Water Development Report, pp. 76.

NOAA National Centers for Environmental information, Climate at a Glance: County Time Series, published April 2019, retrieved on April 22, 2019 from <https://www.ncdc.noaa.gov/cag/>

Postigo, C., Martinez, D., Grondona, S., and Miglioranza, K. 2018. Groundwater Pollution: Sources, Mechanisms, and Prevention: Encyclopedia of the Anthropocene, pp. 87–96.

Prickett, T. A., T. C. Naymik, and C.G. Lonquist. 1981. A “random walk” solute transport model for selected groundwater quality evaluations. Illinois State Water Survey, Bulletin 65, pp. 103.

Sheppard, S., Long, J., and Sanipelli, B. 2009. Solid/liquid partition coefficients (Kd) for selected soils and sediments at Forsmark and Laxemar-Simpevarp: Gustav Sohlenius Geological Survey of Sweden, pp. 1–72.

Srinivasan, P., and J. W. Mercer. 1988. Simulation of biodegradation and sorption processes in ground water. Ground Water 26, no. 4:475-87.

Stenzel, H. B. 1938. The geology of Leon County, Texas: Texas Univ. Pub. 3818, 295 p.

Texas Water Development Board (TWBD). 2003. Water for Texas – 2003. Document No. GP-7-1.

Travis, C. C., and E. L. Etnier. 1981. A survey of sorption relationships for reactive solutes in soil. Journal of Environmental Quality 10, no. 1:8-17.

Watkins, Joseph D. 2018. Mercury in Big Cypress Bayou and Caddo Lake Watersheds in Marian and Harrison Counties, Texas.

Wendlandt, E. A., and Knebel, G. M. 1929. Lower Claiborne of East Texas, with special reference to Mount Sylvan dome and salt movements: Am. Assoc. Petroleum Geologists Bull., v. 13, no. 12, pp. 1347-1375.

Wood, W. W., T. P. Kramer, and P. P. Hem, Jr. 1990. Intergranular diffusion: An important mechanism influencing solute transport in classic aquifers. *Science* 247 (March, 30): 1569-72.

APPENDIX A

DATA INVENTORY

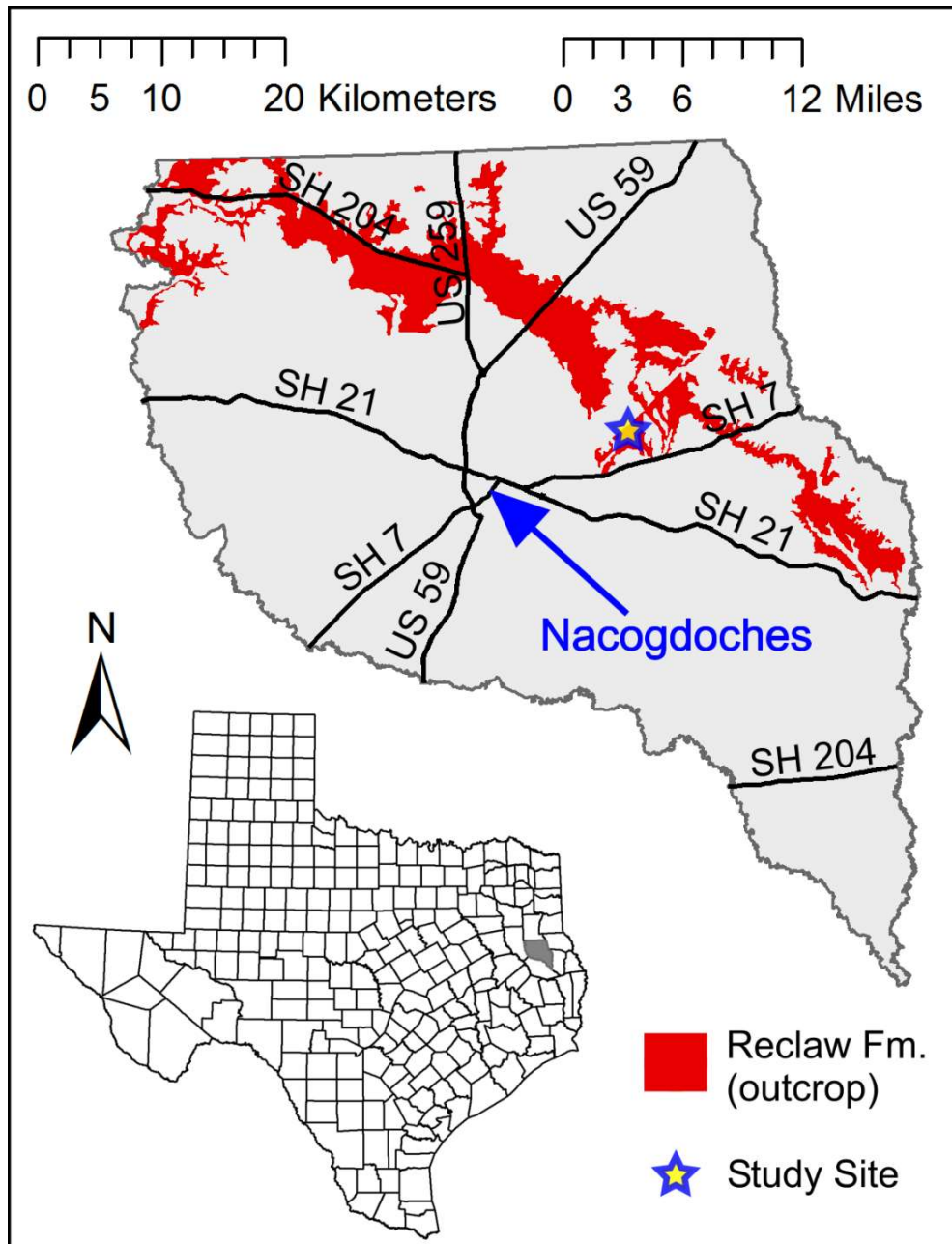


Figure A1. Location of the study area within the Reklaw Formation in Nacogdoches County, Texas. Outcrop area of Reklaw Formation is shown in red; study site is represented by the star east of Nacogdoches, Texas.

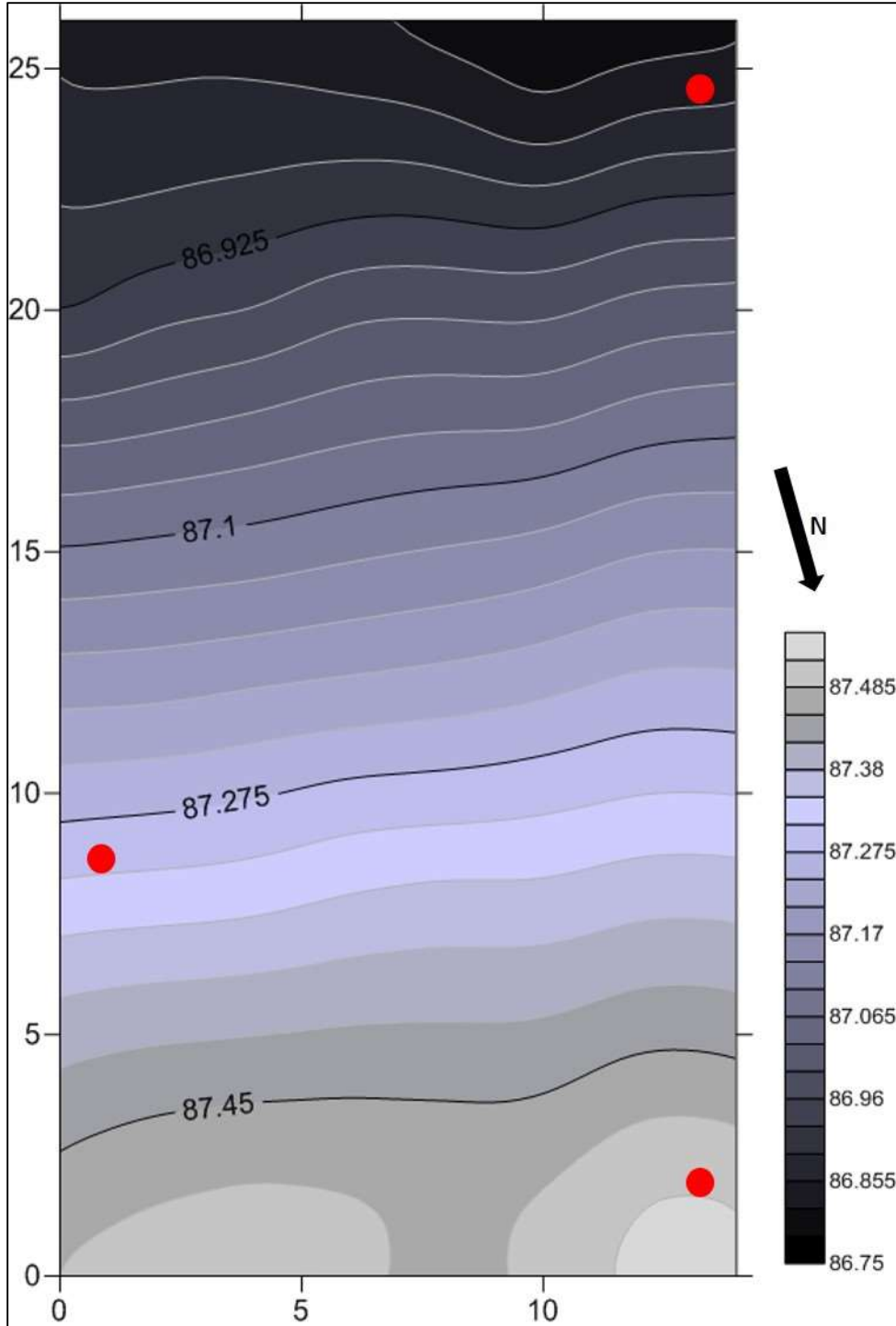


Figure A2. Contoured elevation map (meters) of the study grid with red circles representing the three wells.

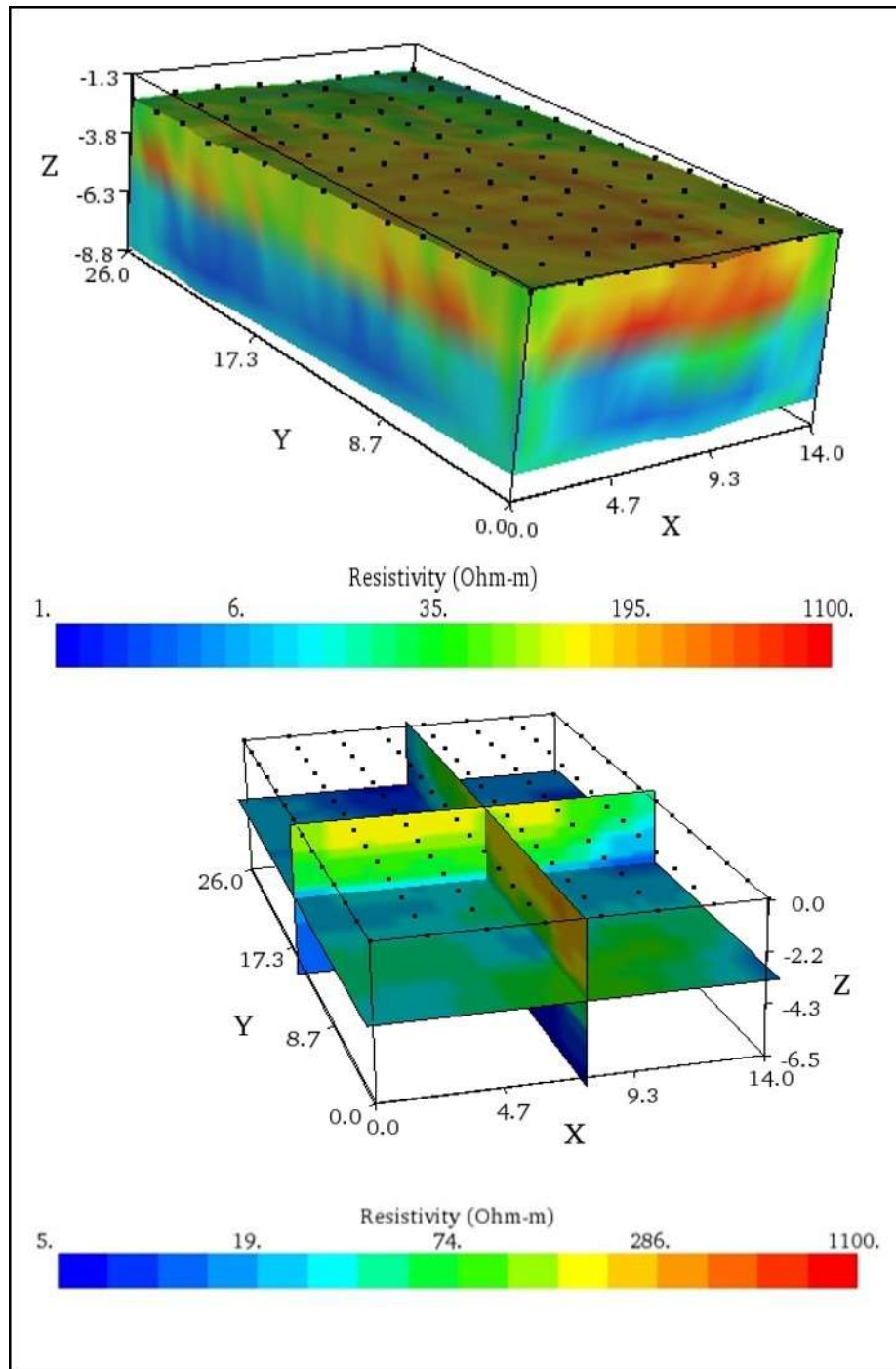


Figure A3. Initial (Day 1) Inverted resistivity section and dynamic slices (RMS = 7.1%, L2 norm = 1.1, Iteration = 8).

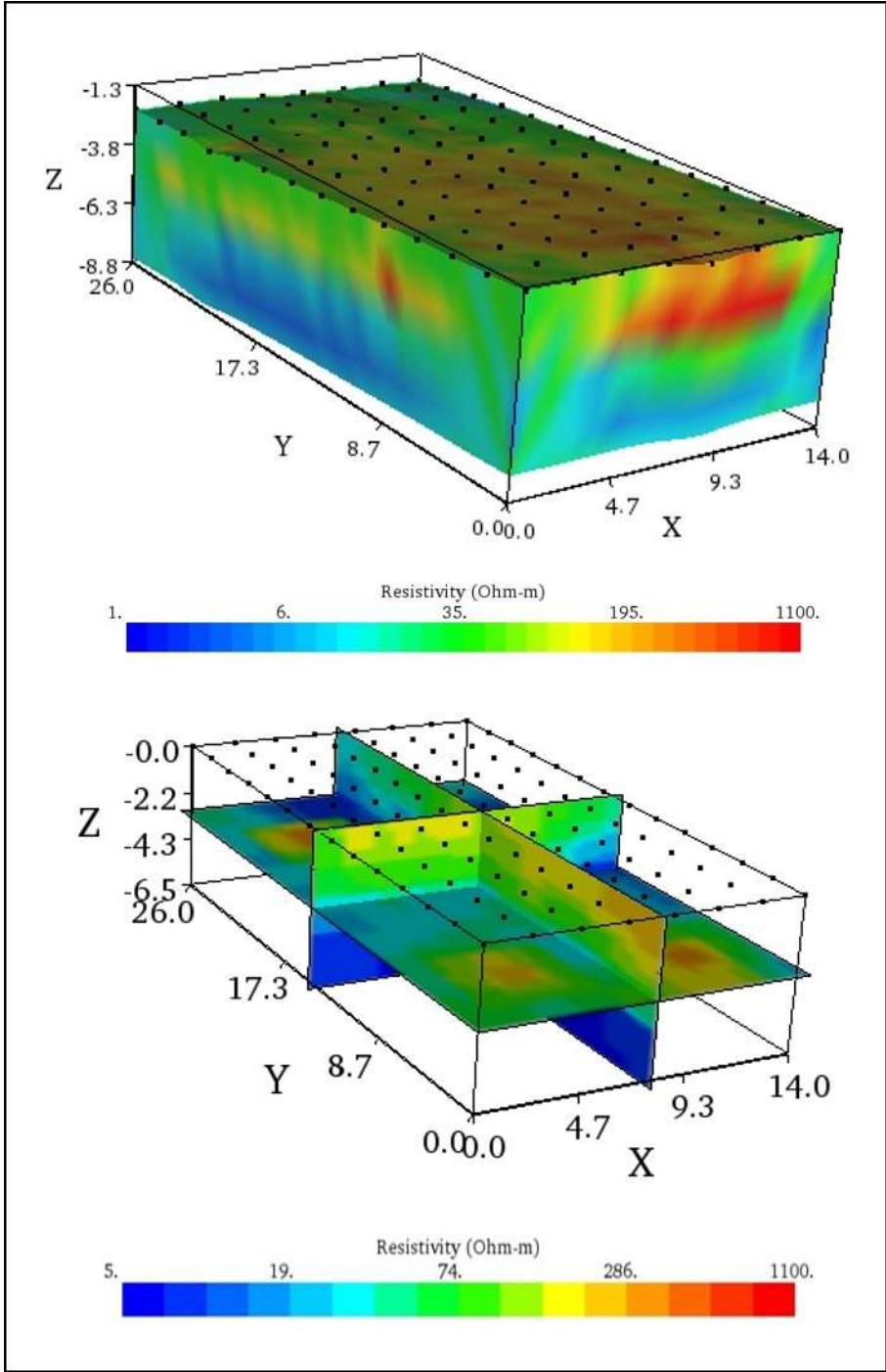


Figure A4. Initial (Day 2) Inverted resistivity section and dynamic slices (RMS = 6.7%, L2 norm = 1.0, Iteration = 8).

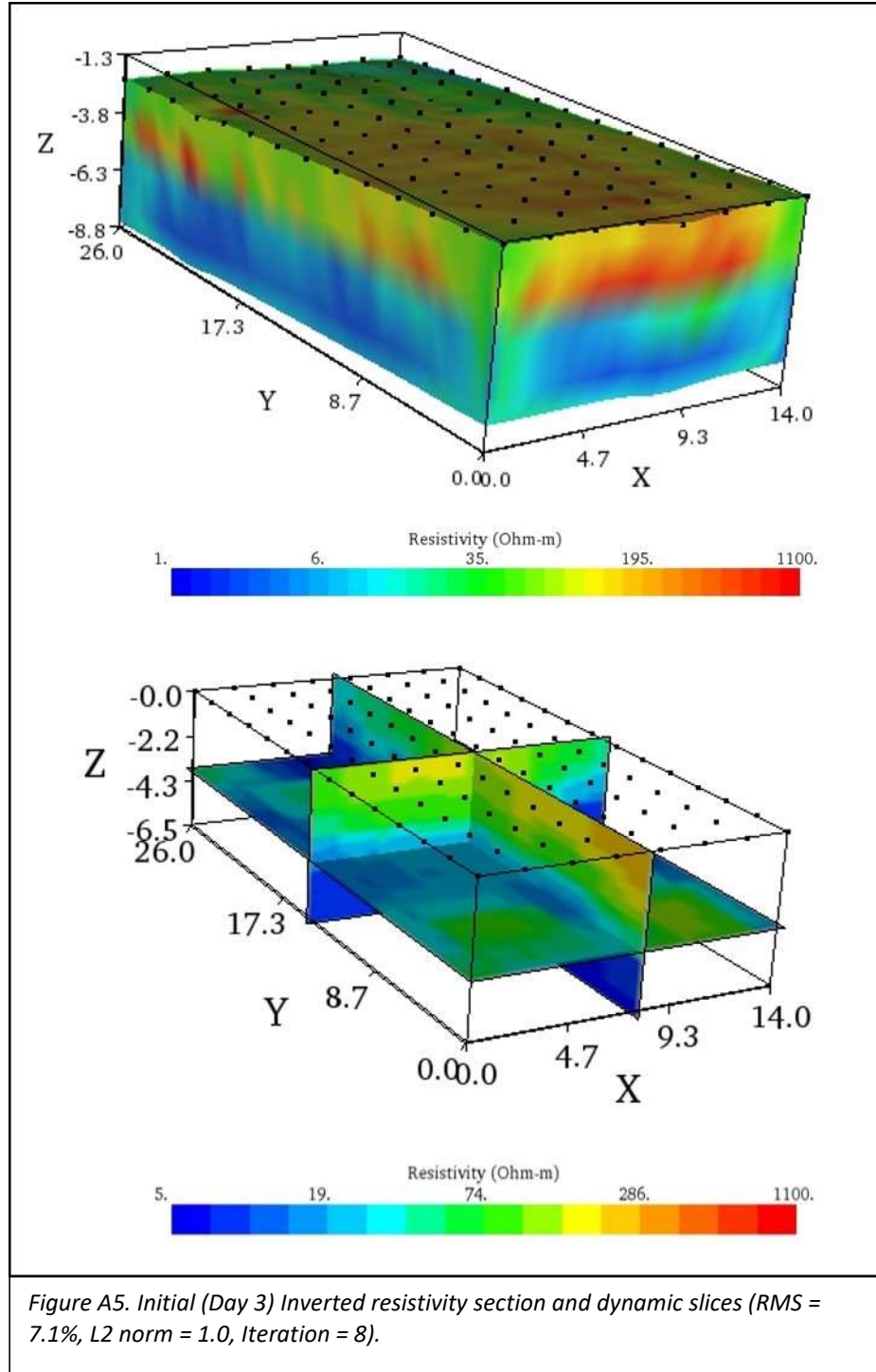


Figure A5. Initial (Day 3) Inverted resistivity section and dynamic slices (RMS = 7.1%, L2 norm = 1.0, Iteration = 8).

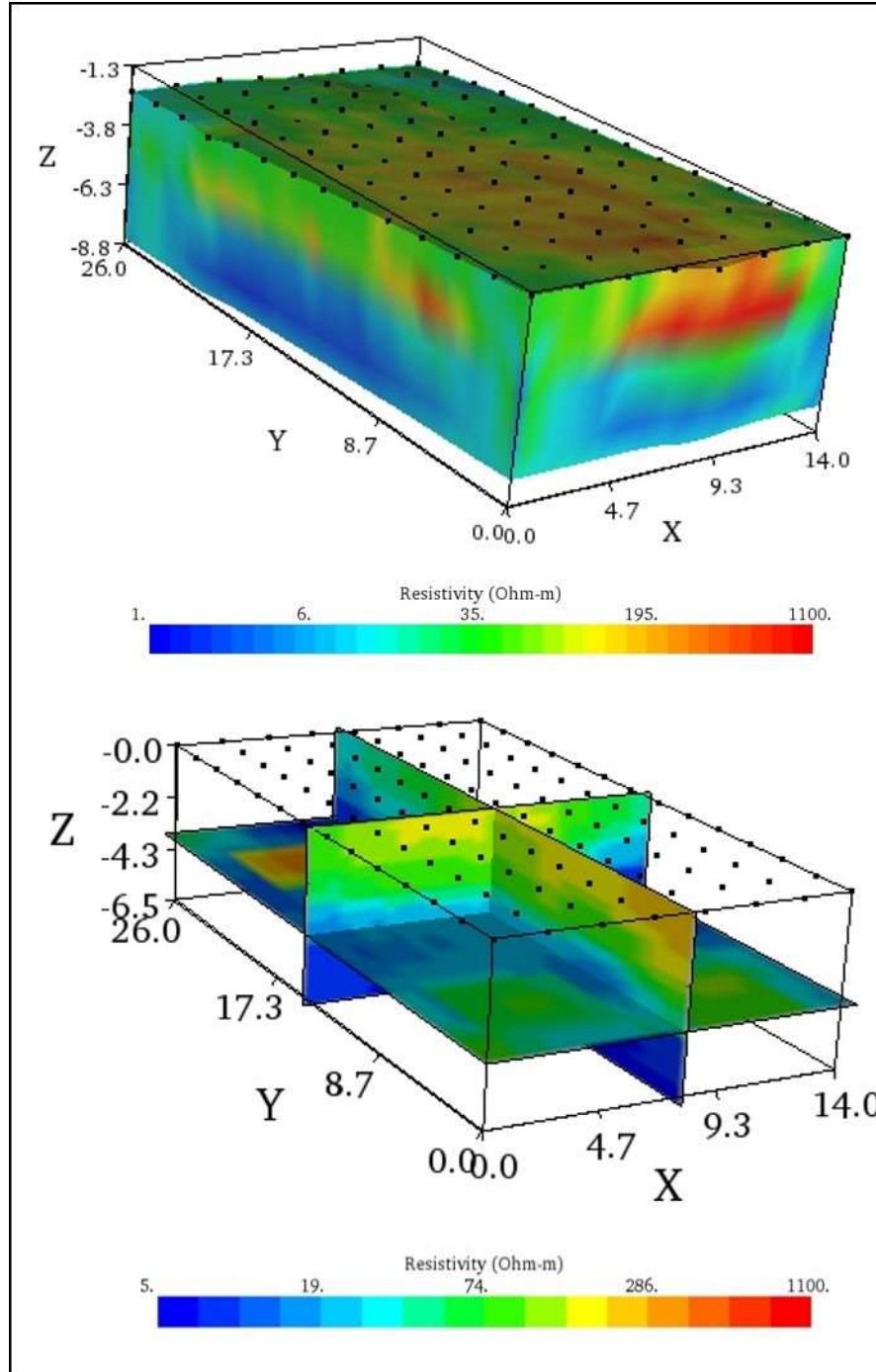


Figure A6. Initial (Day 4) Inverted resistivity section and dynamic slices (RMS = 7.6%, L2 norm = 1.2, Iteration = 8).

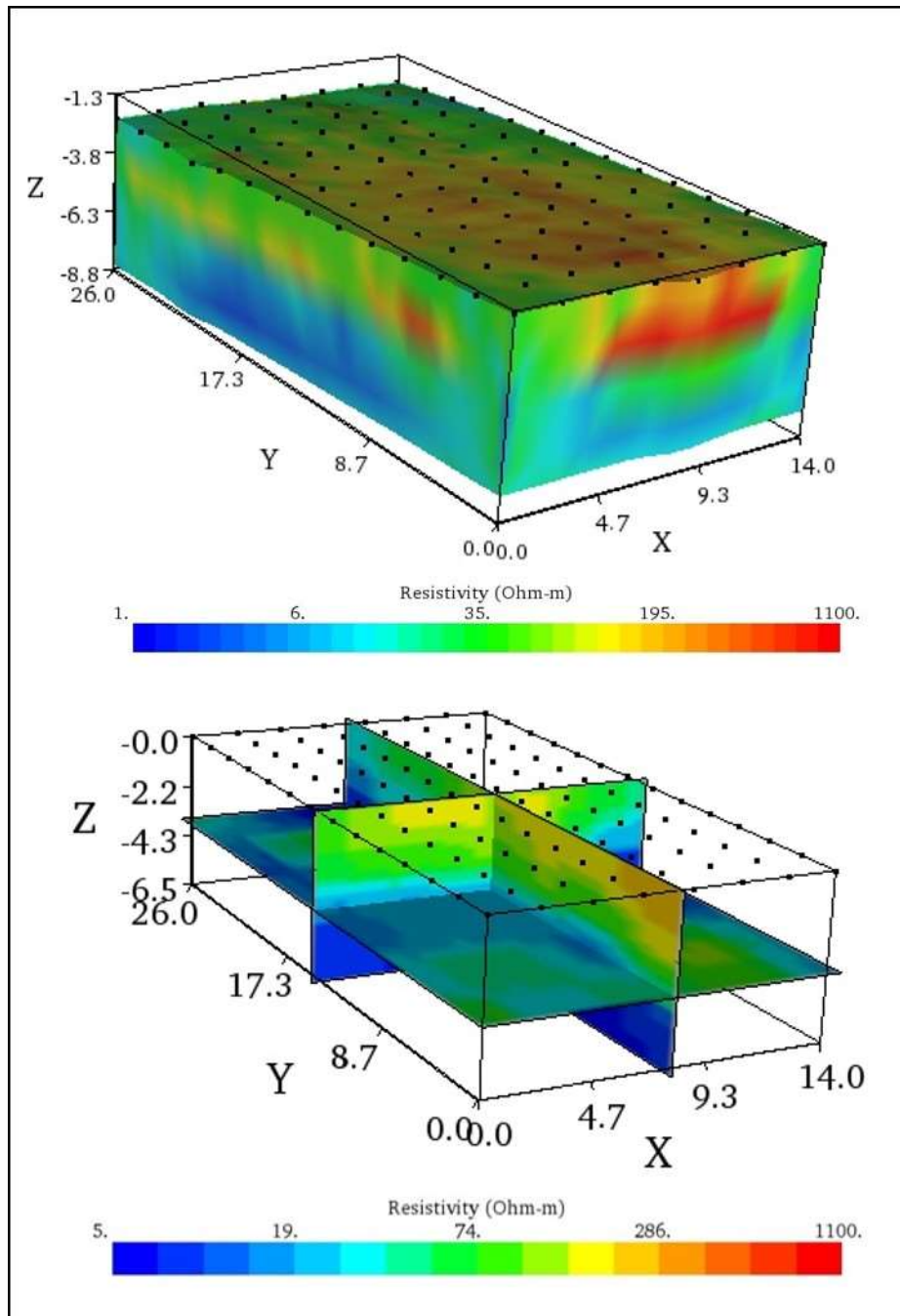


Figure A7. 5-Day Inverted resistivity section and dynamic slices (RMS = 7.8%, L2 norm = 1.2, Iteration = 8).

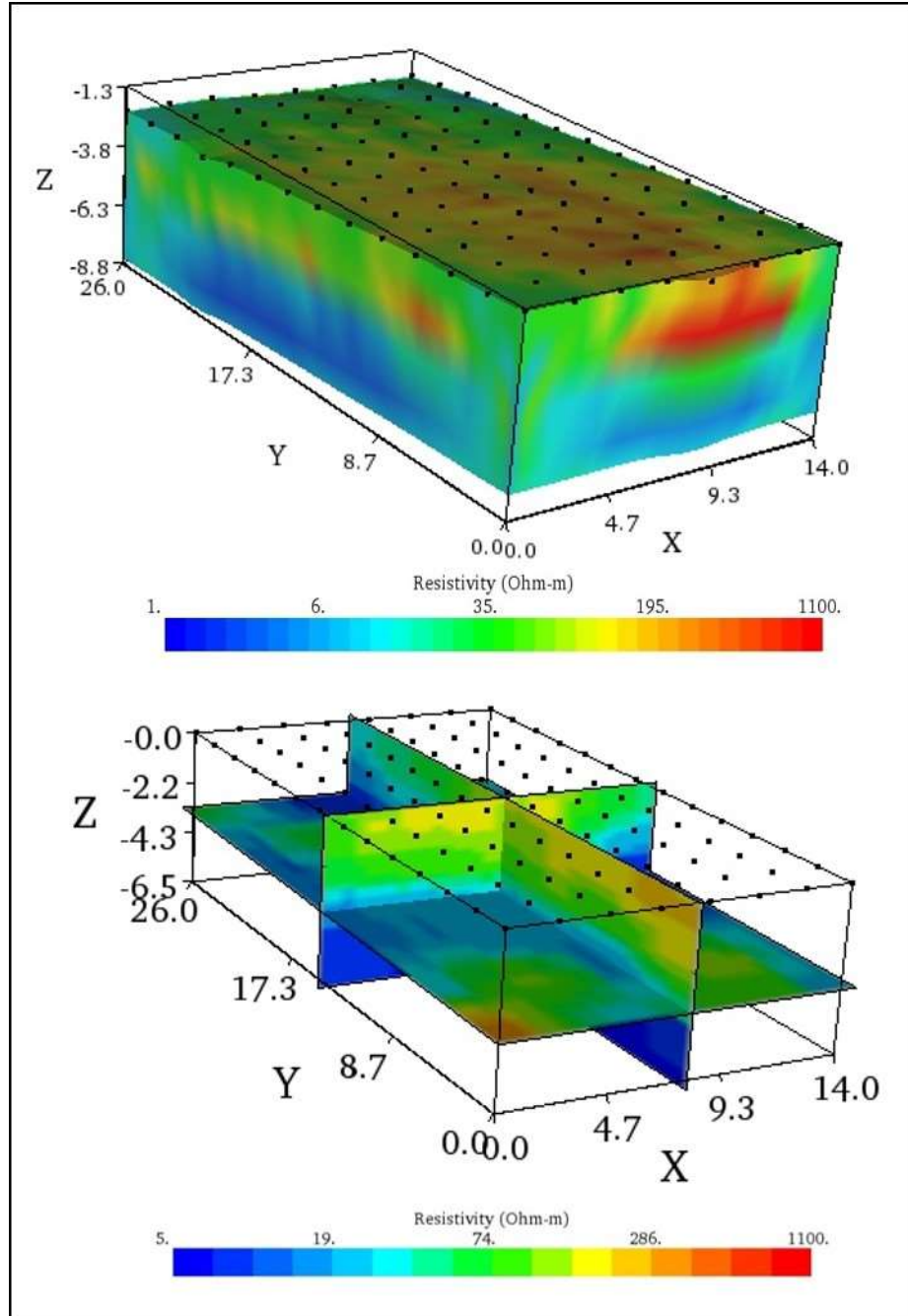


Figure A8. 6-Day Inverted resistivity section and dynamic slices (RMS = 7.4%, L2 norm = 1.2, Iteration = 8).

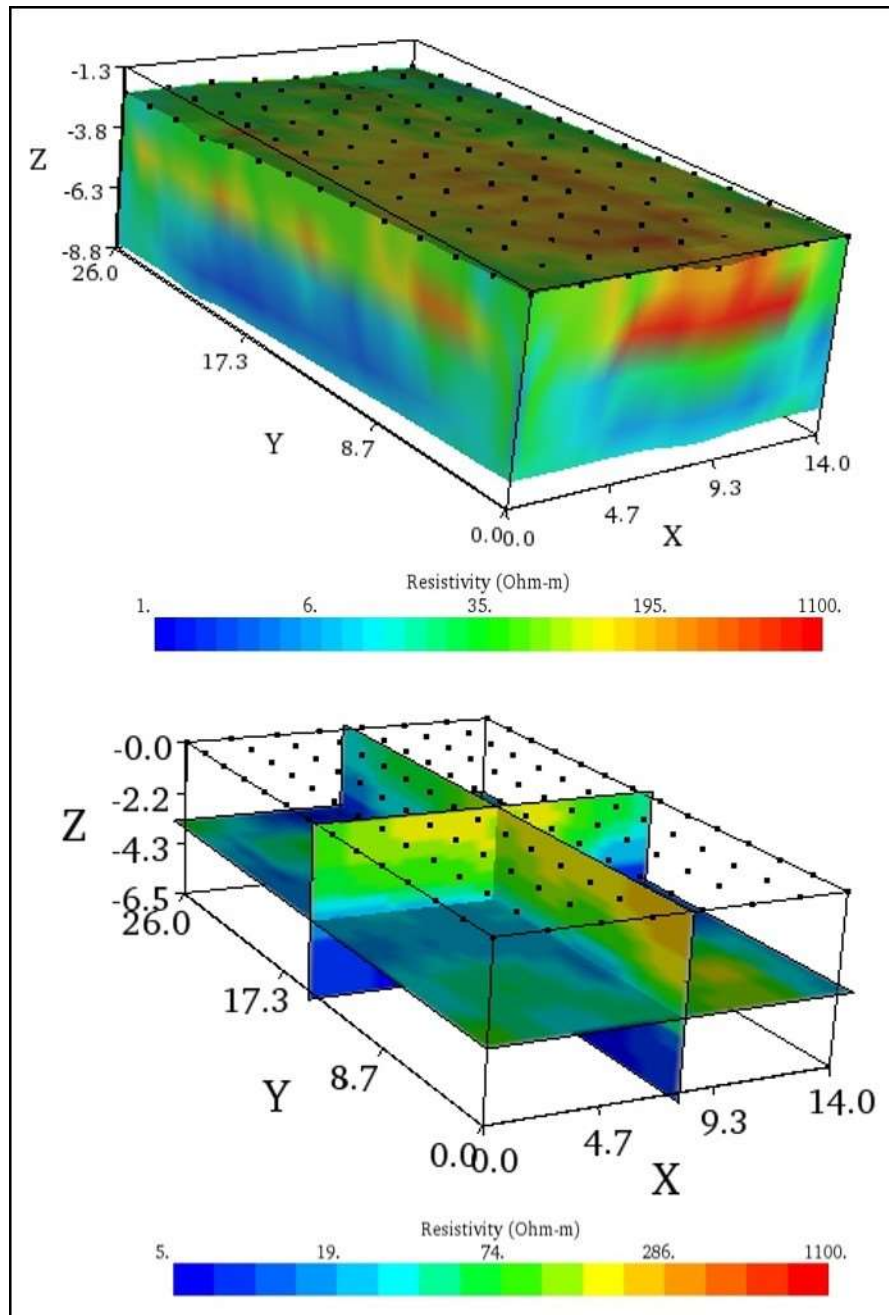


Figure A9. 7-Day Inverted resistivity section and dynamic slices (RMS = 7.9%, L2 norm = 1.3, Iteration = 8).

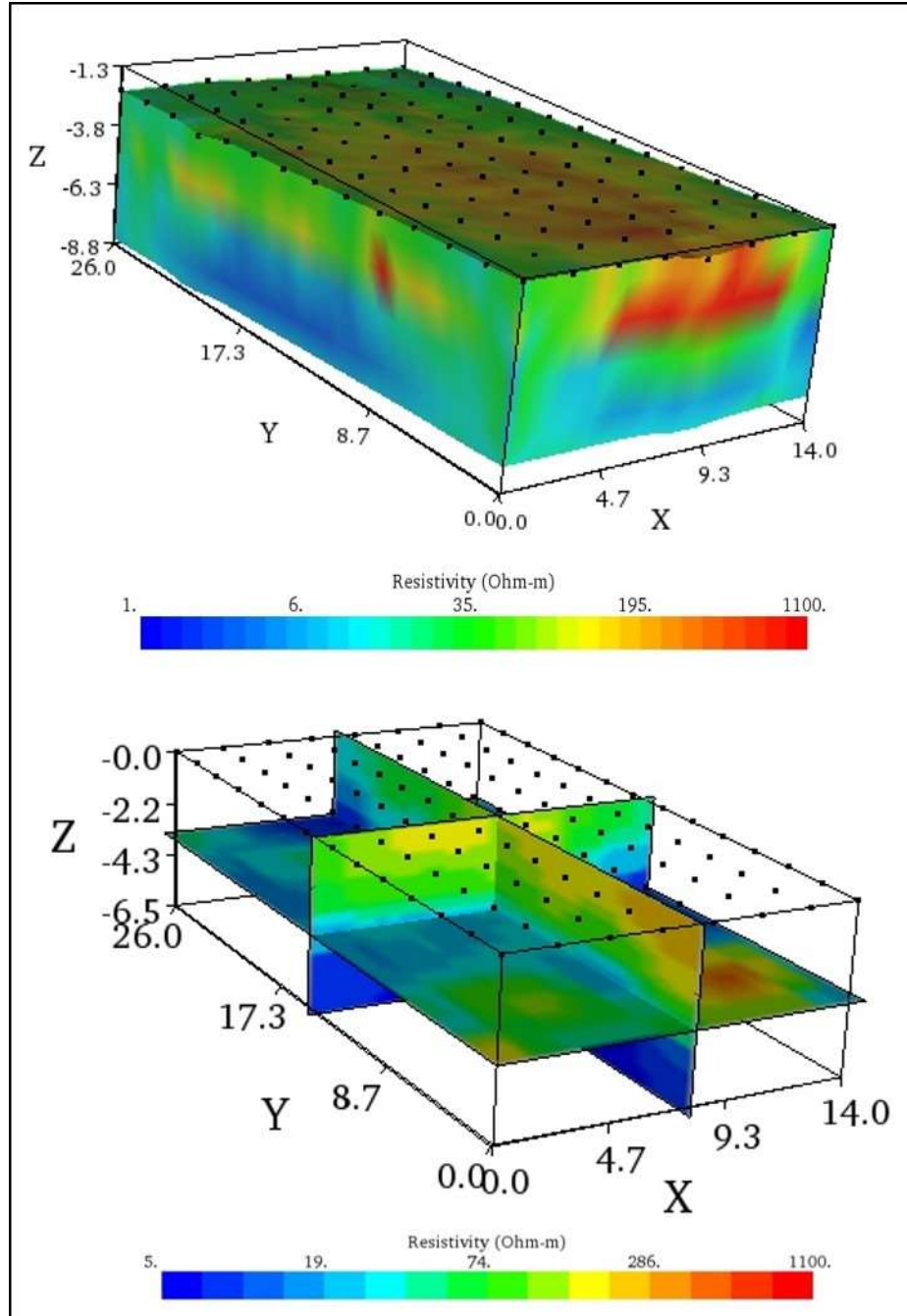


Figure A10. 8-Day Inverted resistivity section and dynamic slices (RMS = 7.2%, L2 norm = 1.1, Iteration = 8).

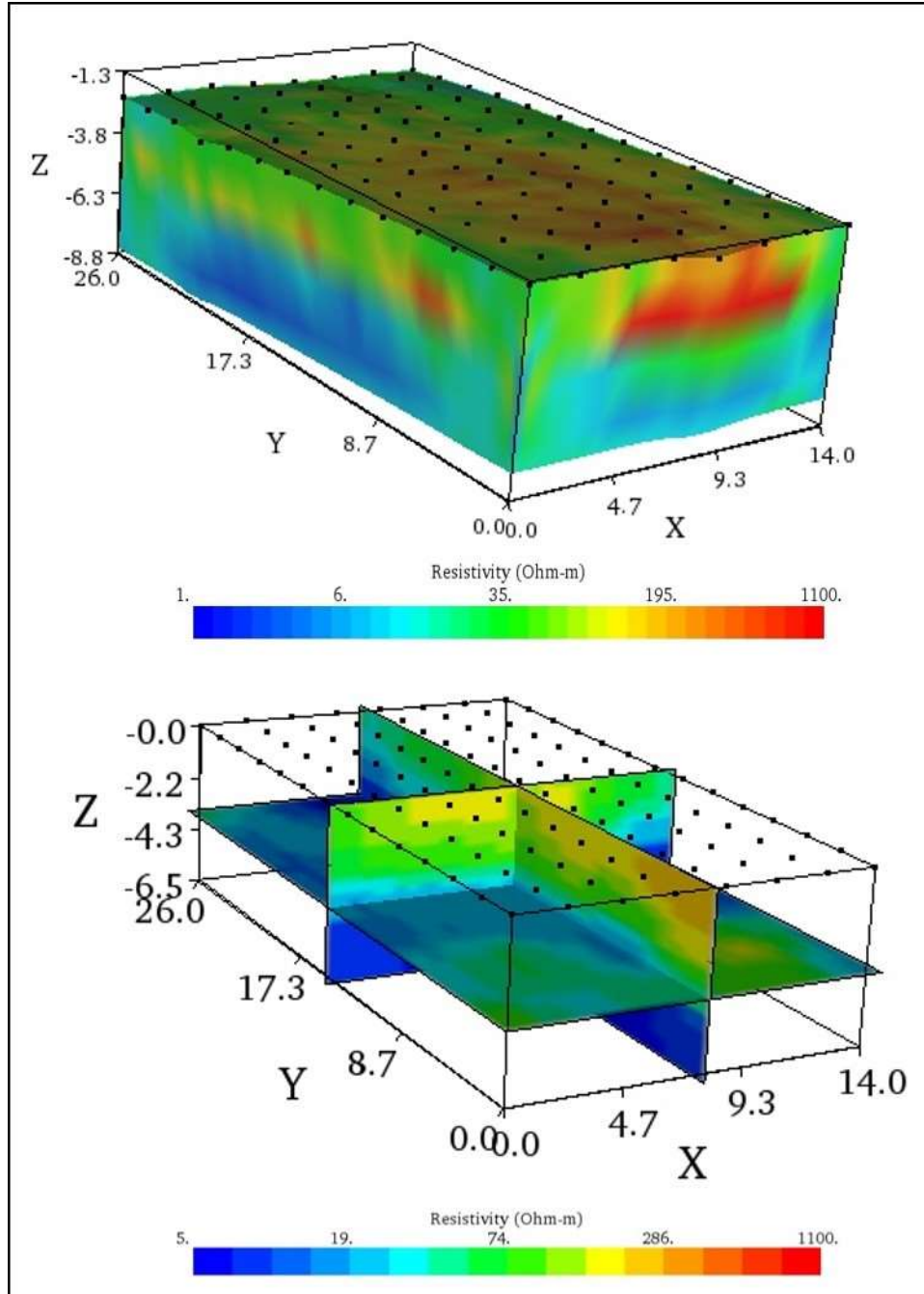


Figure A11. 9-Day Inverted resistivity section and dynamic slices (RMS = 7.8%, L2 norm = 1.2, Iteration = 8).

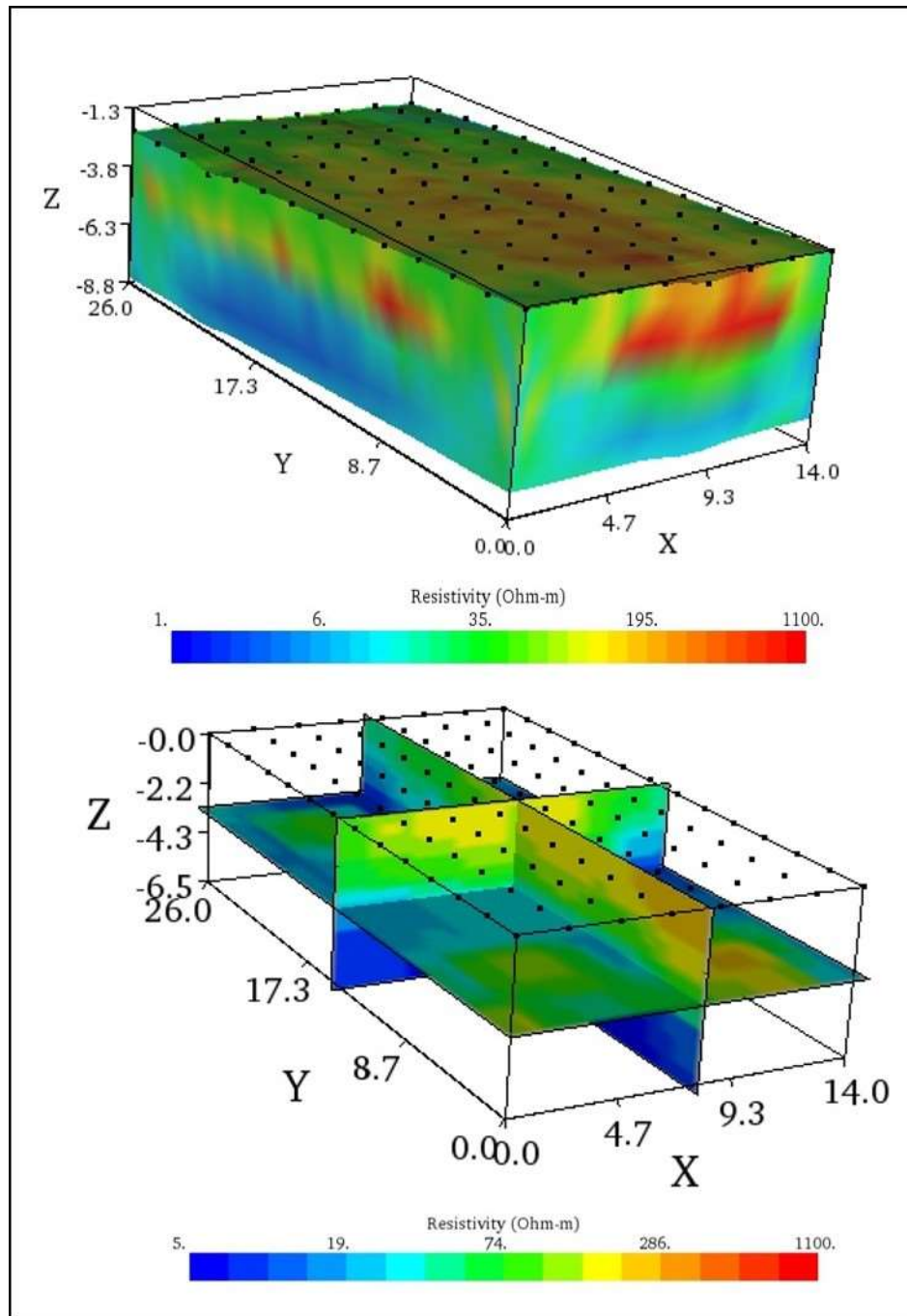


Figure A12. 10-Day Inverted resistivity section and dynamic slices (RMS = 7.4%, L2 norm = 1.1, Iteration = 8).

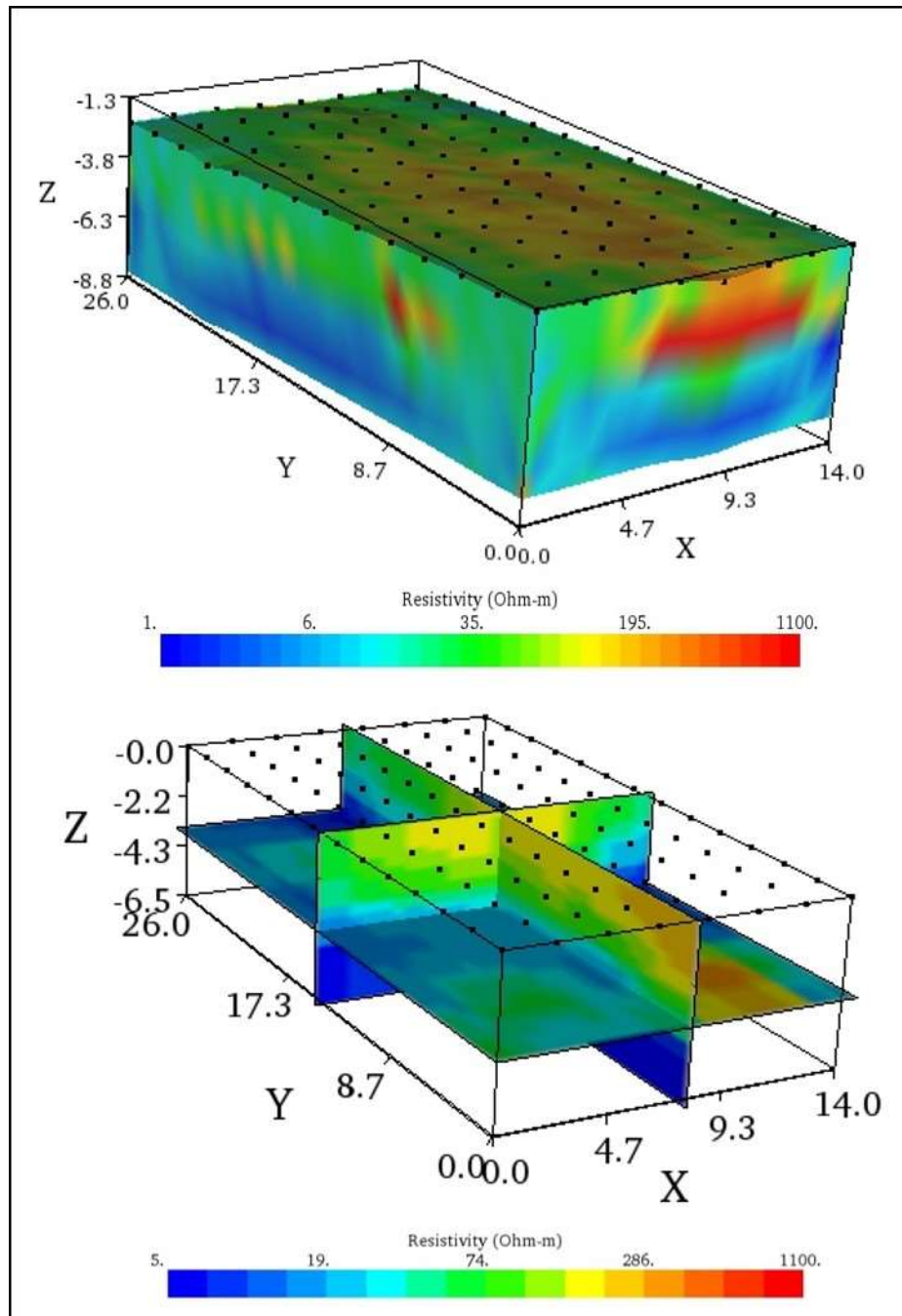


Figure A13. 11-Day Inverted resistivity section and dynamic slices (RMS = 7.2%, L2 norm = 1.1, Iteration = 8).

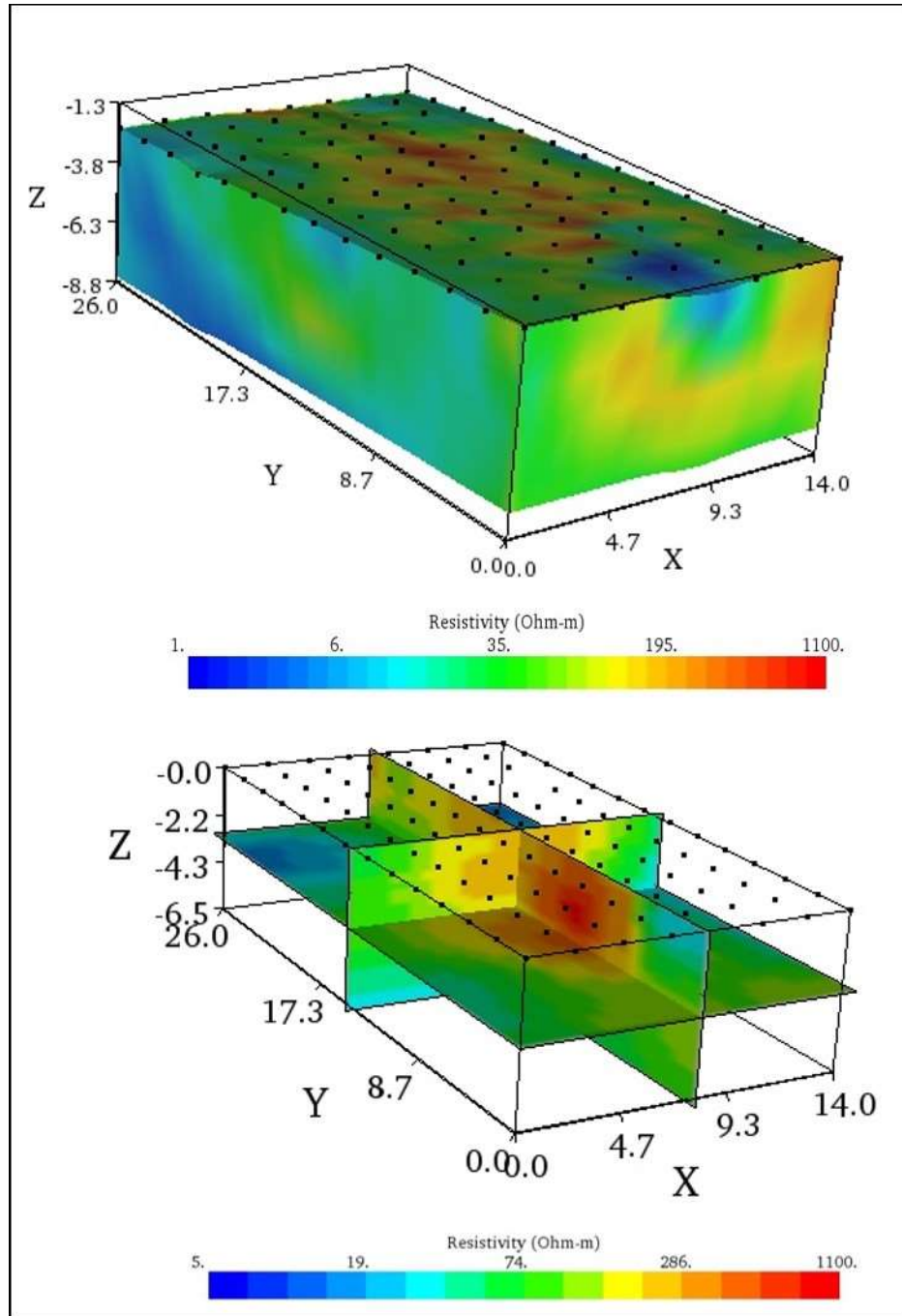


Figure A14. 12-Day Inverted resistivity section and dynamic slices (RMS = 4.0%, L2 norm = 1.4, Iteration = 8).

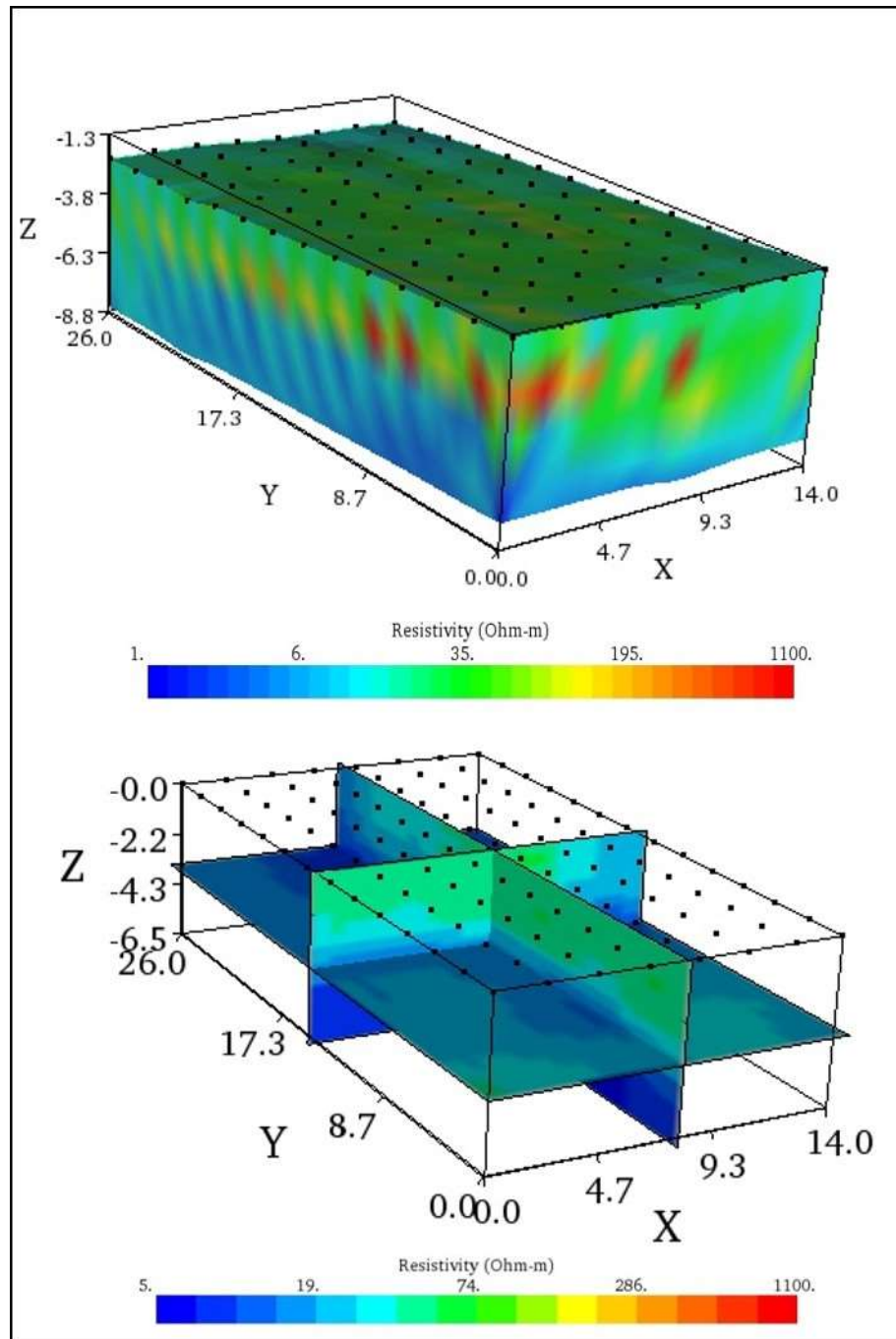


Figure A15. 9-Day Inverted resistivity section and dynamic slices (RMS = 6.7%, L2 norm = 0.9, Iteration = 8).

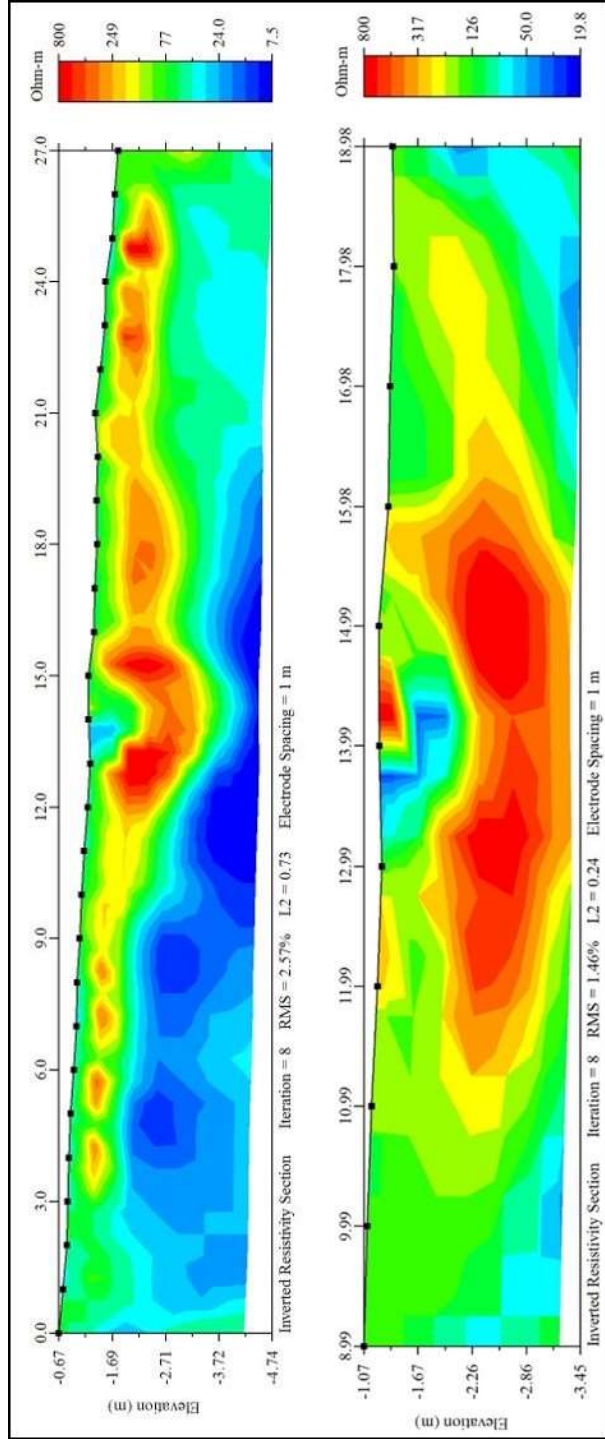


Figure A16. 15-day inverted resistivity section and refined resistivity section (RMS = 2.57%, L2 Norm = 0.73, Iteration = 8).

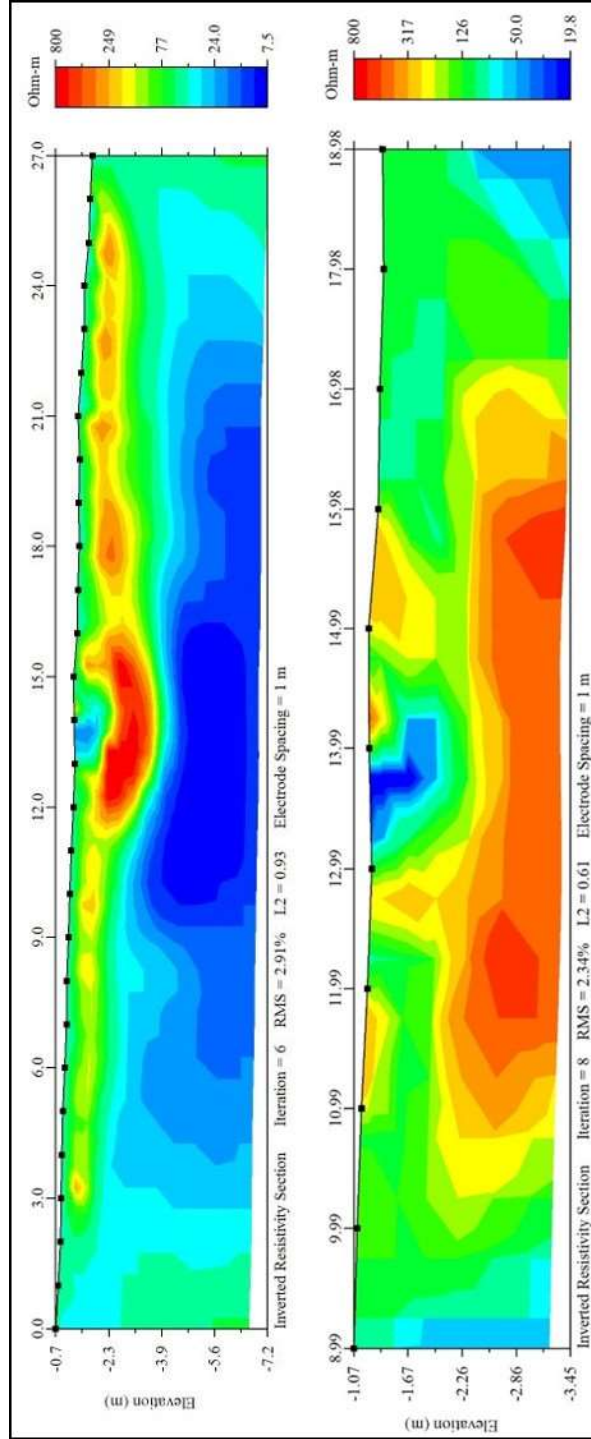


Figure A17. 45-day inverted resistivity section and refined resistivity section (RMS = 2.44%, L2 Norm = 0.65, Iteration = 8).

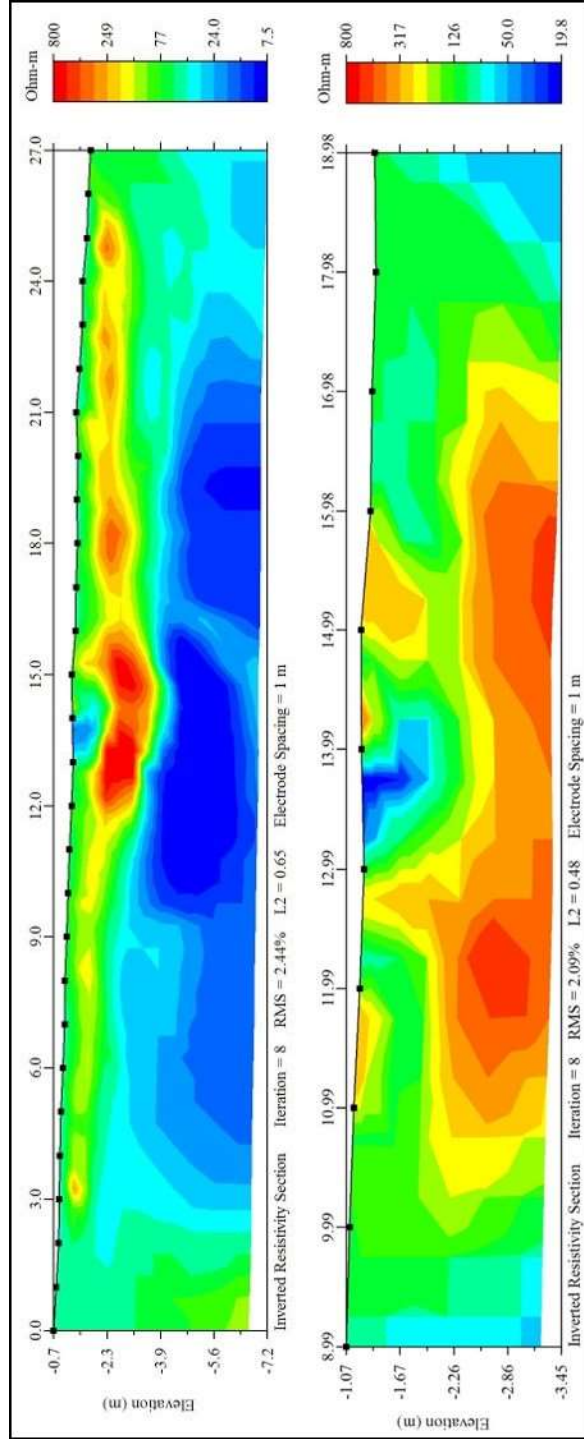


Figure A18. 75-day inverted resistivity section and refined resistivity section (RMS = 2.91%, L2 Norm = 0.93, Iteration = 8).

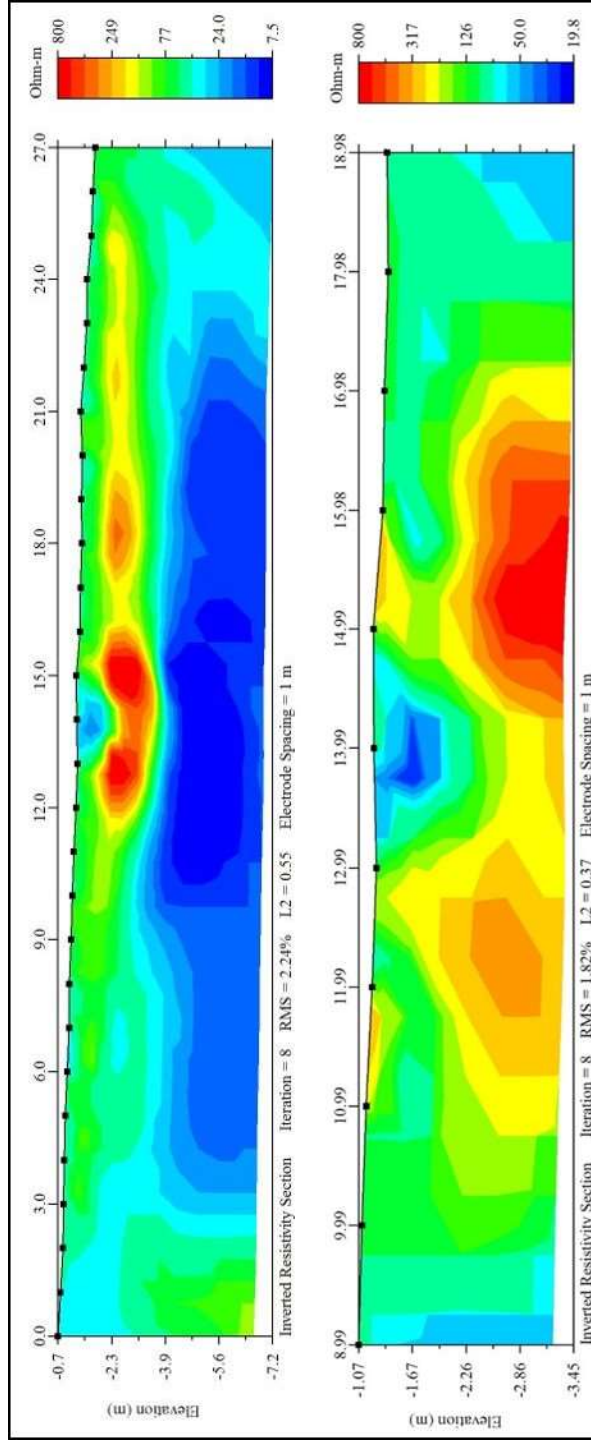


Figure A19. 105-day inverted resistivity section and refined resistivity section (RMS = 2.24%, L2 Norm = 0.55, Iteration = 8).

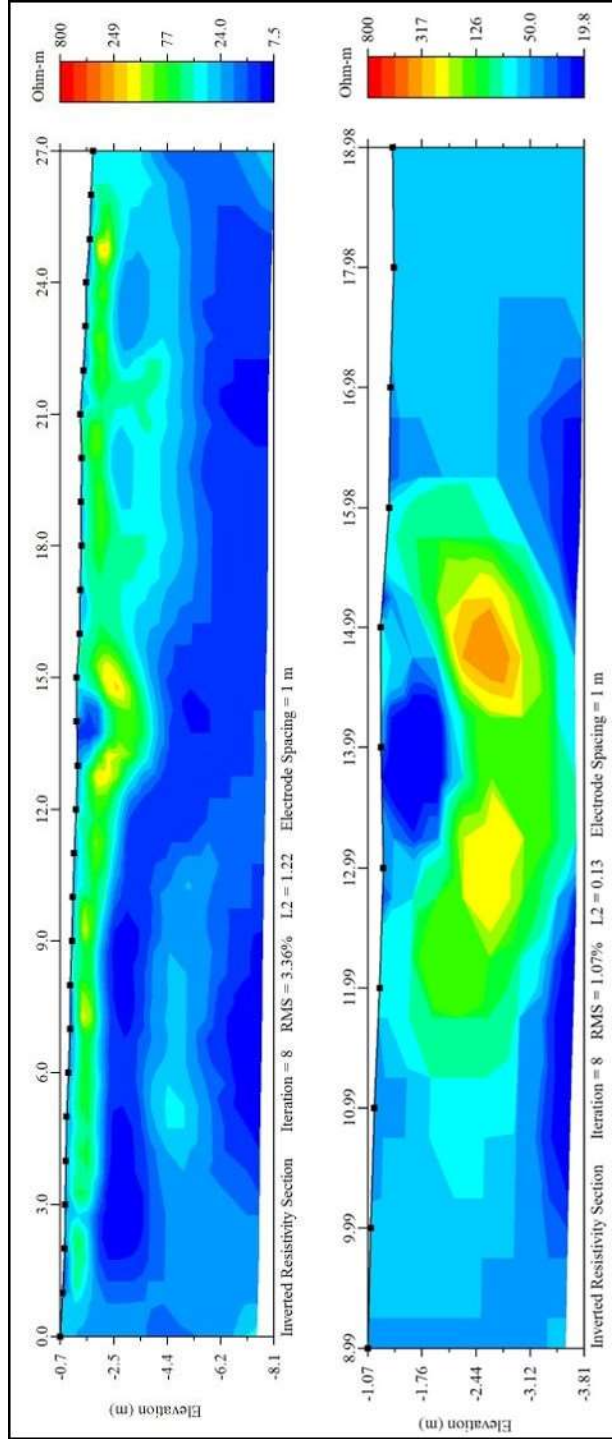


Figure A20. 135-day inverted resistivity section and refined resistivity section (RMS = 3.66%, L2 Norm = 1.22, iteration = 8).

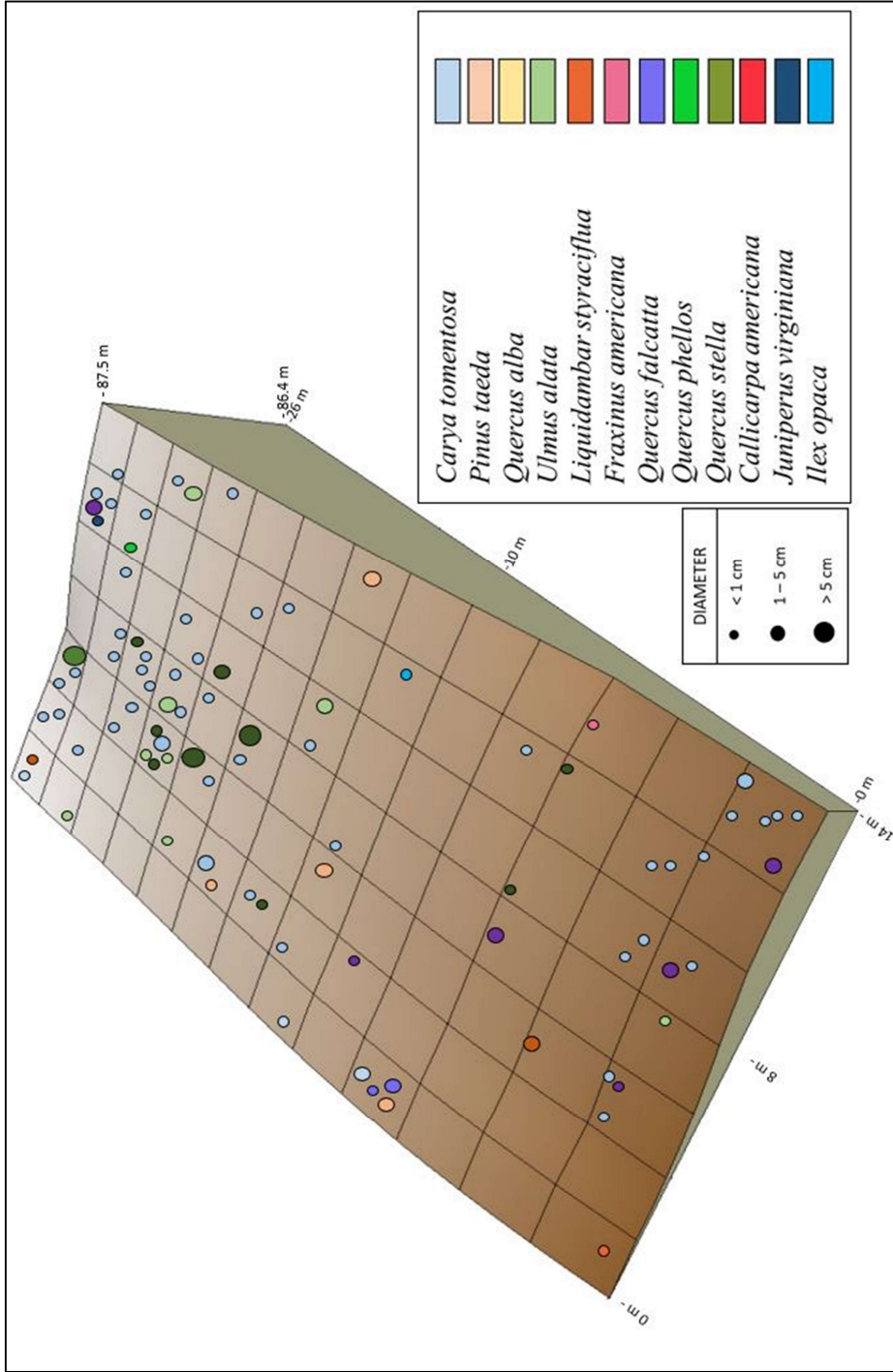


Figure A21. Location and size distribution of tree trunk measured at chest height.

Table A-1. Slug tests administered to each well, including the data, the amount of water delivered, and the rate at which the well recovered (cm/sec).

Slug Tests (cm/sec)		
Date:	Well #1	
1/28/2019	1.0L	5.25E-06
7/10/2018	1.0L	8.2690E-06
	2.0L	7.9360E-06
Date:	Well #2	
1/21/2019	0.5L	1.3202E-05
	0.5L	8.1090E-06
7/10/2018	1.0L	3.3742E-04
	2.0L	4.4796E-04
Date:	Well #3	
1/22/2019	0.5L	2.1227E-04
	1.0L	1.9048E-04
7/10/2018	1.0L	1.6871E-04
	2.0L	1.7206E-04
	Average	
	Well#1	7.1517E-06
	Well #2	2.0167E-04
	Well #3	1.8588E-04

Table A-2. Infiltration tests conducted in four locations and represented by J1, J2, J3, and J4.

Infiltration Test											
J1	1st Run	J2	1st Run	J3	1st Run	J4	1st Run	J3	1st Run	J4	1st Run
5cm	2:52.95	5cm	3:10.36	15min	6.4	15min	10	15min	6.4	15min	10
5cm	8:55.85	5cm	8:26.19	15min	2.8	15min	7.6	15min	2.8	15min	7.6
5cm	9:32.16	5cm	14:03:57	15min	0.2	15min	5.4	15min	0.2	15min	5.4
	2nd Run		2nd Run		2nd Run		2nd Run		2nd Run		2nd Run
5cm	4:48.65	5cm	5:07.14	15min	7.3	15min	10.6	15min	7.3	15min	10.6
5cm	10:07.98	5cm	13:09.28	15min	3.9	15min	8.6	15min	3.9	15min	8.6
5cm	18:42.13	5cm	22:16.78	15min	2.4	15min	6.5	15min	2.4	15min	6.5
	3rd Run		3rd Run		3rd Run		3rd Run		3rd Run		3rd Run
5cm	5:20.74	5cm	5:33.66	15min	7.5	15min	11	15min	7.5	15min	11
5cm	11:16.72	5cm	14:22.64	15min	4.1	15min	9.1	15min	4.1	15min	9.1
5cm	21:51.99	5cm	26:53.32	15min	2.1	15min	7.4	15min	2.1	15min	7.4
	4th Run		4th Run		4th Run		4th Run		4th Run		4th Run
5cm	4:14.21	5cm	6:24.87	15min	8	15min	11.2	15min	8	15min	11.2
5cm	12:30.91	5cm	16:14.30	15min	4.8	15min	9.6	15min	4.8	15min	9.6
5cm	27:05.40	5cm	29:08.45	15min	2.5	15min	7.9	15min	2.5	15min	7.9
	Average		Average		Average		Average		Average		Average
5cm	4:19.16	5cm	5:04.16	15min	7.3	15min	10.7	15min	7.3	15min	10.7
5cm	10:48.12	5cm	13:03.12	15min	3.9	15min	8.725	15min	3.9	15min	8.725
5cm	19:17.75	5cm	23:05.50	15min	1.8	15min	6.8	15min	1.8	15min	6.8
	cm/min		cm/min		cm/min		cm/min		cm/min		cm/min
5cm	1.158212	5cm	0.986777	15min	0.48666	15min	0.71333	15min	0.48666	15min	0.71333
5cm	0.462963	5cm	0.383142	15min	0.26	15min	0.581667	15min	0.26	15min	0.581667
5cm	0.259292	5cm	0.216638	15min	0.12	15min	0.453333	15min	0.12	15min	0.453333

Table A-3. Particle size analysis conducted on sediments located at site 1 (close to “injection” site).

Sample(cm)	Temp (°F)	Particle-Size Analysis: Hydrometer Method												
		30 sec	60 sec	3 min	10 min	30 min	60 min	90 min	120 min	720 min				
S1-10	69.08	46.216	46.216	45.216	41.216	38.216	38.216	38.216	36.216	36.216	36.216	36.216	31.216	
S1-20	68.72	47.144	46.144	46.144	44.144	43.144	41.144	41.144	39.144	39.144	39.144	39.144	36.144	
S1-30	68.18	49.036	46.036	45.036	43.036	40.036	39.036	39.036	38.036	38.036	38.036	38.036	34.036	
S1-40	68	46.000	46.000	45.000	44.000	43.000	41.000	41.000	40.000	40.000	40.000	37.000	37.000	
S1-50	68.36	46.072	45.072	44.072	44.072	41.072	40.072	40.072	40.072	40.072	39.072	39.072	36.072	
S1-60	68.72	46.144	46.144	46.144	44.144	43.144	41.144	41.144	40.144	40.144	40.144	40.144	37.144	
S1-70	68	46.000	46.000	44.000	41.000	39.000	38.000	38.000	37.000	37.000	36.000	36.000	32.000	
S1-80	69.08	45.216	44.216	44.216	41.216	39.216	38.216	38.216	37.216	37.216	37.216	37.216	33.216	
S1-90	69.44	45.288	44.288	44.288	40.288	38.288	37.288	37.288	36.288	36.288	36.288	36.288	29.288	
S1-100	69.8	45.360	44.360	43.360	41.360	38.360	36.360	36.360	34.360	34.360	34.360	34.360	29.360	
S1-110	69.8	45.108	44.108	43.108	41.108	38.108	37.108	37.108	35.108	35.108	34.108	34.108	31.108	
S1-120	69.8	45.108	44.108	43.108	40.108	38.108	36.108	36.108	34.108	34.108	33.108	33.108	31.108	
S1-130	69.8	45.108	44.108	43.108	39.108	37.108	34.108	34.108	33.108	33.108	33.108	33.108	29.108	
S1-140	69.8	44.108	43.108	42.108	39.108	36.108	35.108	35.108	34.108	34.108	32.108	32.108	28.108	
S1-150	69.8	44.108	43.108	41.108	39.108	37.108	34.108	34.108	33.108	33.108	32.108	32.108	27.108	
S1-160	69.8	46.108	44.108	43.108	41.108	39.108	38.108	38.108	37.108	37.108	37.108	37.108	32.108	
S1-170	68	43.108	41.108	39.108	37.108	36.108	34.108	34.108	33.108	33.108	32.108	32.108	28.108	
S1-180	67.1	38.928	37.928	37.928	35.928	33.928	31.928	31.928	31.928	31.928	30.928	30.928	26.928	
S1-190	67.28	31.964	28.964	28.964	26.964	26.964	24.964	24.964	22.964	22.964	22.964	22.964	20.964	
S1-200	67.28	30.964	28.964	25.964	21.964	20.964	19.964	19.964	18.964	18.964	18.964	18.964	15.964	
S1-210	67.28	31.964	28.964	26.964	26.964	24.964	22.964	22.964	21.964	21.964	21.964	21.964	19.964	
S1-220	67.46	33.000	32.000	31.000	29.000	28.000	27.000	27.000	27.000	27.000	27.000	27.000	23.000	
S1-230	67.64	31.036	28.036	27.036	25.036	25.036	23.036	23.036	23.036	23.036	22.036	22.036	19.036	
S1-240	69.8	27.928	26.928	25.928	23.928	22.928	22.928	22.928	21.928	21.928	21.928	21.928	17.928	
S1-250	69.8	28.928	26.928	25.928	23.928	21.928	21.928	21.928	21.928	21.928	20.928	20.928	17.928	

Table A-4. Particle size analysis conducted on sediments located at site 2 (near well #1).

Particle-Size Analysis: Hydrometer Method												
Sample (cm)	Temp (°F)	30 sec	60 sec	3 min	10 min	30 min	60 min	90 min	120 min	720 min		
S2-10	69.8	37.928	34.928	32.928	26.928	25.928	19.928	17.928	16.928	14.928		
S2-20	69.8	41.928	40.928	39.928	37.928	33.928	31.928	31.928	29.928	26.928		
S2-30	69.8	44.928	43.928	41.928	38.928	36.928	33.928	32.928	32.928	28.928		
S2-40	69.8	44.928	43.928	41.928	40.928	37.928	36.928	34.928	34.928	31.928		
S2-50	69.8	46.928	45.928	45.928	44.928	41.928	41.928	40.928	39.928	38.928		
S2-60	69.8	46.928	45.928	45.928	45.928	43.928	43.928	43.928	41.928	38.928		
S2-70	67.1	46.820	45.820	45.820	44.820	43.820	40.820	40.820	39.820	36.820		
S2-80	67.28	46.856	45.856	45.856	44.856	43.856	40.856	39.856	39.856	36.856		
S2-90	67.28	46.856	45.856	45.856	44.856	43.856	40.856	39.856	39.856	37.856		
S2-100	67.28	45.856	45.856	44.856	43.856	40.856	39.856	38.856	38.856	35.856		
S2-110	66.92	42.784	40.784	39.784	38.784	37.784	36.784	35.784	33.784	30.784		
S2-120	66.92	42.784	39.784	38.784	36.784	33.784	32.784	31.784	31.784	27.784		
S2-130	67.1	35.820	32.820	31.820	28.820	27.820	26.820	25.820	24.820	20.820		
S2-140	66.92	33.784	28.784	27.784	26.784	25.784	22.784	22.784	22.784	19.784		
S2-150	69.26	27.432	26.432	26.432	25.432	23.432	22.432	21.432	20.432	17.432		
S2-160	66.92	27.964	26.964	25.964	24.964	24.964	22.964	21.964	20.964	18.964		
S2-170	66.38	30.856	28.856	26.856	25.856	25.856	22.856	22.856	21.856	19.856		
S2-180	66.38	32.856	31.856	30.856	28.856	27.856	25.856	25.856	24.856	21.856		
S2-190	66.38	31.856	27.856	26.856	25.856	24.856	22.856	22.856	21.856	19.856		
S2-200	67.1	28.000	26.000	25.000	23.000	22.000	21.000	20.000	20.000	17.000		
S2-210	67.46	26.072	23.072	21.072	20.072	19.072	17.072	16.072	16.072	14.072		
S2-220	67.46	27.072	25.072	22.072	20.072	17.072	15.072	15.072	14.072	11.072		

Table A-5. Particle size analysis conducted on sediments located at site 3 (near the back right of the grid).

Particle-Size Analysis: Hydrometer Method												
Sample (cm)	Temp (°F)	30 sec	60 sec	3 min	10 min	30 min	60 min	90 min	120 min	720 min		
S3-10	69.62	36.964	33.964	31.964	25.964	21.964	18.964	15.964	14.964	10.964		
S3-20	69.8	44.000	43.000	40.000	38.000	36.000	33.000	32.000	31.000	27.000		
S3-30	69.8	45.000	44.000	44.000	40.000	39.000	37.000	36.000	36.000	32.000		
S3-40	69.8	44.000	43.000	40.000	38.000	37.000	34.000	33.000	33.000	29.000		
S3-50	69.8	44.000	43.000	40.000	38.000	36.000	33.000	32.000	31.000	28.000		
S3-60	69.8	44.000	41.000	40.000	38.000	36.000	33.000	32.000	32.000	28.000		
S3-70	69.26	39.892	38.892	37.892	36.892	33.892	31.892	28.892	28.892	25.892		
S3-80	69.26	44.892	43.892	42.892	39.892	37.892	35.892	33.892	33.892	30.892		
S3-90	69.26	43.892	42.896	42.892	39.892	37.892	36.892	35.892	32.892	30.892		
S3-100	69.08	43.856	42.856	40.856	38.856	36.856	35.856	33.856	31.856	28.856		
S3-110	69.08	44.856	43.856	43.856	39.856	37.856	36.856	35.856	32.856	30.856		
S3-120	69.08	44.856	43.856	43.856	39.856	37.856	36.856	35.856	32.856	30.856		
S3-130	71.06	44.676	43.676	41.676	38.676	37.676	34.676	33.676	33.676	37.676		
S3-140	71.06	44.676	41.676	41.676	40.676	38.676	37.676	36.676	36.676	32.676		
S3-150	71.06	43.676	41.676	41.676	40.676	39.676	38.676	37.676	37.676	33.676		
S3-160	71.06	44.676	41.676	41.676	40.676	39.676	38.676	37.676	36.676	33.676		
S3-170	71.06	39.676	38.676	37.676	34.676	33.676	32.676	31.676	31.676	28.676		
S3-180	71.06	37.676	34.676	33.676	32.676	31.676	28.676	28.676	28.676	26.676		
S3-190	71.06	34.676	32.676	29.676	28.676	27.676	26.676	26.676	25.676	23.676		
S3-200	71.06	33.676	31.676	29.676	28.676	27.676	26.676	26.676	25.676	22.676		
S3-210	71.06	27.676	25.676	23.676	22.676	20.676	20.676	19.676	19.676	16.676		
S3-220	71.06	27.676	25.676	23.676	22.676	20.676	20.676	20.676	17.676	16.676		
S3-230	71.06	31.676	28.676	27.676	25.676	23.676	23.676	22.676	21.676	19.676		

Table A-6. Particle size analysis for percentage of sand, silt, and clay. Located at site 1 (close to “injection” site).

Sample(cm)	Particle-Size Analysis: Hydrometer Method (Percentage)										
	30 sec	60 sec	3 min	10 min	30 min	60 min	90 min	120 min	720 min		
S1-10	92.33966	92.33966	90.34166	82.34965	76.35564	76.35564	72.35964	72.35964	62.36963		
S1-20	94.19381	92.1958	92.1958	88.1998	86.2018	82.20579	78.20979	78.20979	72.21578		
S1-30	97.97403	91.98002	89.98202	85.98601	79.99201	77.99401	75.996	75.996	68.004		
S1-40	91.90809	91.90809	89.91009	87.91209	85.91409	81.91808	79.92008	73.92607	73.92607		
S1-50	92.05195	90.05395	88.05594	88.05594	82.06194	80.06394	80.06394	78.06593	72.07193		
S1-60	92.1958	92.1958	92.1958	88.1998	86.2018	82.20579	80.20779	80.20779	74.21379		
S1-70	91.90809	91.90809	87.91209	81.91808	77.92208	75.92408	73.92607	71.92807	63.93606		
S1-80	90.34166	88.34366	88.34366	82.34965	78.35365	76.35564	74.35764	74.35764	66.36563		
S1-90	90.48551	88.48751	88.48751	80.4955	76.4995	74.5015	72.5035	72.5035	58.51748		
S1-100	90.62937	88.63137	86.63337	82.63736	76.64336	72.64735	68.65135	68.65135	58.66134		
S1-110	90.12587	88.12787	86.12987	82.13387	76.13986	74.14186	70.14585	68.14785	62.15385		
S1-120	90.12587	88.12787	86.12987	80.13586	76.13986	72.14386	68.14785	66.14985	62.15385		
S1-130	90.12587	88.12787	86.12987	78.13786	74.14186	68.14785	66.14985	66.14985	58.15784		
S1-140	88.12787	86.12987	84.13187	78.13786	72.14386	70.14585	68.14785	64.15185	56.15984		
S1-150	88.12787	86.12987	82.13387	78.13786	74.14186	68.14785	66.14985	64.15185	54.16184		
S1-160	92.12388	88.12787	86.12987	82.13387	78.13786	76.13986	74.14186	74.14186	64.15185		
S1-170	86.12987	82.13387	78.13786	74.14186	72.14386	68.14785	66.14985	64.15185	56.15984		
S1-180	77.77822	75.78022	75.78022	71.78422	67.78821	63.79221	63.79221	61.79421	53.8022		
S1-190	63.86414	57.87013	57.87013	53.87413	53.87413	49.87812	45.88212	45.88212	41.88611		
S1-200	61.86613	57.87013	51.87612	43.88412	41.88611	39.88811	37.89011	37.89011	31.8961		
S1-210	63.86414	57.87013	53.87413	53.87413	49.87812	45.88212	43.88412	43.88412	39.88811		
S1-220	65.93407	63.93606	61.93806	57.94206	55.94406	53.94605	53.94605	53.94605	45.95405		
S1-230	62.00999	56.01598	54.01798	50.02198	50.02198	46.02597	46.02597	44.02797	38.03397		
S1-240	55.8002	53.8022	51.8042	47.80819	45.81019	45.81019	43.81219	43.81219	35.82018		
S1-250	57.7982	53.8022	51.8042	47.80819	43.81219	43.81219	43.81219	41.81419	35.82018		

Table A-7. Particle size analysis for percentage of sand, silt, and clay. Located at site 2 (near well #1).

Sample (cm)	Particle-Size Analysis: Hydrometer Method (percentage)										
	30 sec	60 sec	3 min	10 min	30 min	60 min	90 min	120 min	720 min		
S2-10	75.78022	69.78621	65.79021	53.8022	51.8042	39.81618	35.82018	33.82218	29.82617		
S2-20	83.77223	81.77423	79.77622	75.78022	67.78821	63.79221	63.79221	59.7962	53.8022		
S2-30	89.76623	87.76823	83.77223	77.77822	73.78222	67.78821	65.79021	65.79021	57.7982		
S2-40	89.76623	87.76823	83.77223	81.77423	75.78022	73.78222	69.78621	69.78621	63.79221		
S2-50	93.76224	91.76424	91.76424	89.76623	83.77223	83.77223	81.77423	79.77622	77.77822		
S2-60	93.76224	91.76424	91.76424	91.76424	87.76823	87.76823	87.76823	83.77223	77.77822		
S2-70	93.54645	91.54845	91.54845	89.55045	87.55245	81.55844	81.55844	79.56044	73.56643		
S2-80	93.61838	91.62038	91.62038	89.62238	87.62438	81.63037	79.63237	79.63237	73.63836		
S2-90	93.61838	91.62038	91.62038	89.62238	87.62438	81.63037	79.63237	79.63237	75.63636		
S2-100	91.62038	91.62038	89.62238	87.62438	81.63037	79.63237	77.63437	77.63437	71.64036		
S2-110	85.48252	81.48651	79.48851	77.49051	75.49251	73.49451	71.4965	67.5005	61.50649		
S2-120	85.48252	79.48851	77.49051	73.49451	67.5005	65.5025	63.5045	63.5045	55.51249		
S2-130	71.56843	65.57443	63.57642	57.58242	55.58442	53.58641	51.58841	49.59041	41.5984		
S2-140	67.5005	57.51049	55.51249	53.51449	51.51648	45.52248	45.52248	45.52248	39.52847		
S2-150	54.80919	52.81119	52.81119	50.81319	46.81718	44.81918	42.82118	40.82318	34.82917		
S2-160	55.87213	53.87413	51.87612	49.87812	49.87812	45.88212	43.88412	41.88611	37.89011		
S2-170	61.65035	57.65435	53.65834	51.66034	51.66034	45.66633	45.66633	43.66833	39.67233		
S2-180	65.64635	63.64835	61.65035	57.65435	55.65634	51.66034	51.66034	49.66234	43.66833		
S2-190	63.64835	55.65634	53.65834	51.66034	49.66234	45.66633	45.66633	43.66833	39.67233		
S2-200	55.94406	51.94805	49.95005	45.95405	43.95604	41.95804	39.96004	39.96004	33.96603		
S2-210	52.09191	46.0979	42.1019	40.1039	38.10589	34.10989	32.11189	32.11189	28.11588		
S2-220	54.08991	50.09391	44.0999	40.1039	34.10989	30.11389	30.11389	28.11588	22.12188		

Table A-8. Particle size analysis for percentage of sand, silt, and clay. Located at site 2 (near back right of study grid).

Sample (cm)	Particle-Size Analysis: Hydrometer Method (Percentage)										
	30 sec	60 sec	3 min	10 min	30 min	60 min	90 min	120 min	720 min		
S3-10	73.85415	67.86014	63.86414	51.87612	43.88412	37.89011	31.8961	29.8981	21.90609		
S3-20	87.91209	85.91409	79.92008	75.92408	71.92807	65.93407	63.93606	61.93806	53.94605		
S3-30	89.91009	87.91209	87.91209	79.92008	77.92208	73.92607	71.92807	71.92807	63.93606		
S3-40	87.91209	85.91409	79.92008	75.92408	73.92607	67.93207	65.93407	65.93407	57.94206		
S3-50	87.91209	85.91409	79.92008	75.92408	71.92807	65.93407	63.93606	61.93806	55.94406		
S3-60	87.91209	81.91808	79.92008	75.92408	71.92807	65.93407	63.93606	63.93606	55.94406		
S3-70	79.7043	77.70629	75.70829	73.71029	67.71628	63.72028	57.72627	57.72627	51.73227		
S3-80	89.69431	87.6963	85.6983	79.7043	75.70829	71.71229	67.71628	67.71628	61.72228		
S3-90	87.6963	85.70629	85.6983	79.7043	75.70829	73.71029	71.71229	65.71828	61.72228		
S3-100	87.62438	85.62637	81.63037	77.63437	73.63836	71.64036	67.64436	63.64835	57.65435		
S3-110	89.62238	87.62438	87.62438	79.63237	75.63636	73.63836	71.64036	65.64635	61.65035		
S3-120	89.62238	87.62438	87.62438	79.63237	75.63636	73.63836	71.64036	65.64635	61.65035		
S3-130	89.26274	87.26474	83.26873	77.27473	75.27672	69.28272	67.28472	67.28472	75.27672		
S3-140	89.26274	83.26873	83.26873	81.27073	77.27473	75.27672	73.27872	73.27872	65.28671		
S3-150	87.26474	83.26873	83.26873	81.27073	79.27273	77.27473	75.27672	75.27672	67.28472		
S3-160	89.26274	83.26873	83.26873	81.27073	79.27273	77.27473	75.27672	73.27872	67.28472		
S3-170	79.27273	77.27473	75.27672	69.28272	67.28472	65.28671	63.28871	63.28871	57.29471		
S3-180	75.27672	69.28272	67.28472	65.28671	63.28871	57.29471	57.29471	57.29471	53.2987		
S3-190	69.28272	65.28671	59.29271	57.29471	55.2967	53.2987	53.2987	51.3007	47.3047		
S3-200	67.28472	63.28871	59.29271	57.29471	55.2967	53.2987	53.2987	51.3007	45.30669		
S3-210	55.2967	51.3007	47.3047	45.30669	41.31069	41.31069	39.31269	39.31269	33.31868		
S3-220	55.2967	51.3007	47.3047	45.30669	41.31069	41.31069	41.31069	35.31668	33.31868		
S3-230	63.28871	57.29471	55.2967	51.3007	47.3047	47.3047	45.30669	43.30869	39.31269		

Table A9A. Solute plume migration in each direction stemming from the “injection” site.

Day/meter	0.1,0.0	0.2,0.0	0.3,0.0	0.4,0.0	0.5,0.0	0.6,0.0
15	3.75046E-05	3.46E-16	1.43E-35	3.52E-71	3.68E-141	2.01E-293
45	4.95E-14	7.71E-37	7.78E-77	1.67E-150	7.75E-296	0
75	8.71E-23	2.28E-57	5.59E-118	1.02E-229	0	0
105	1.72E-31	7.60E-78	4.51E-159	0	0	0
135	3.64E-40	2.70E-98	3.87E-200	0	0	0
Day/meter	0.0,0.1	0.0,0.2	0.0,0.3	0.0,0.4	0.0,0.5	
15	3.01428E-05	1.27E-16	7.66E-37	2.45E-74	1.35E-148	
45	3.96E-14	2.73E-37	3.58E-78	6.89E-154	5.78E-304	
75	6.97E-23	8.01E-58	2.44E-119	3.55E-233	0	
105	1.38E-31	2.65E-78	1.92E-160	0	0	
135	2.91E-40	9.38E-99	1.62E-201	0	0	
Day/meter	0.1,0.1	0.2,0.2	0.3,0.3	0.4,0.4	0.5,0.5	0.6,0.6
15	4.15423E-05	5.96E-16	8.74E-35	7.51E-69	4.79E-135	3.93E-277
45	5.45E-14	1.25E-36	3.67E-76	1.43E-148	6.29E-291	0
75	9.57E-23	3.64E-57	2.42E-117	6.45E-228	0	0
105	1.89E-31	1.20E-77	1.87E-158	3.79E-307	0	0
135	3.99E-40	4.24E-98	1.56E-199	0	0	0
Day/meter	(-),0.1,(-),0.1	(-),0.2,(-),0.2	(-),0.3,(-),0.3	(-),0.4,(-),0.4	(-),0.5,(-),0.5	
15	2.20877E-05	2.97E-17	1.03E-38	3.84E-79	4.30E-160	
45	2.90E-14	6.25E-38	4.31E-80	7.29E-159	0	
75	5.09E-23	1.82E-58	2.84E-121	3.30E-238	0	
105	1.01E-31	5.99E-79	2.19E-162	0	0	
135	2.12E-40	2.12E-99	1.83E-203	0	0	

Table A9B. Solute plume migration in each direction stemming from the “injection” site.

Day/meter	(-)0.1,0.0	(-)0.2,0.0	(-)0.3,0.0	(-)0.4,0.0	(-)0.5,0.0	
15	2.38851E-05	4.07E-17	2.23E-38	2.11E-78	8.44E-159	
45	3.15E-14	9.06E-38	1.21E-79	1.00E-157	0	
75	5.55E-23	2.68E-58	8.71E-121	6.13E-237	0	
105	1.10E-31	8.94E-79	7.02E-162	0	0	
135	2.32E-40	3.17E-99	6.03E-203	0	0	
Day/meter	0.0,(-)0.1	0.0,(-)0.2	0.0,(-)0.3	0.0,(-)0.4	0.0,(-)0.5	
15	3.01428E-05	1.27E-16	7.66E-37	2.45E-74	1.35E-148	
45	3.96E-14	2.73E-37	3.58E-78	6.89E-154	5.78E-304	
75	6.97E-23	8.01E-58	2.44E-119	3.55E-233	0	
105	1.38E-31	2.65E-78	1.92E-160	0	0	
135	2.91E-40	9.38E-99	1.62E-201	0	0	
Day/meter	(-)0.1,0.1	(-)0.2,0.2	(-)0.3,0.3	(-)0.4,0.4	(-)0.5,0.5	
15	2.20877E-05	2.97E-17	1.03E-38	3.84E-79	4.30E-160	
45	2.90E-14	6.25E-38	4.31E-80	7.29E-159	0	
75	5.09E-23	1.82E-58	2.84E-121	3.30E-238	0	
105	1.01E-31	5.99E-79	2.19E-162	0	0	
135	2.12E-40	2.12E-99	1.83E-203	0	0	
Day/meter	0.1,(-)0.1	0.2,(-)0.2	0.3,(-)0.3	0.4,(-)0.4	0.5,(-)0.5	0.6,(-)0.6
15	4.15423E-05	5.96E-16	8.74E-35	7.51E-69	4.79E-135	3.93E-277
45	5.45E-14	1.25E-36	3.67E-76	1.43E-148	6.29E-291	0
75	9.57E-23	3.64E-57	2.42E-117	6.45E-228	0	0
105	1.89E-31	1.20E-77	1.87E-158	3.79E-307	0	0
135	3.99E-40	4.24E-98	1.56E-199	0	0	0

VITA

Kaleb J. Henry graduate from Waxahachie Preparatory Academy in Waxahachie, Texas in the year of 2009. He received a Bachelor of Science in Geology from Wayland Baptist University in the year 2015. Kaleb Henry was admitted to the Graduate School of Stephen F. Austin State University and received a degree of Master of Science in Geology in August of 2019.

Permanent Address: 704 West Marvin Ave.
 Waxahachie, Texas 75165

Style manual designation: Texas Water Journal

This thesis was typed by Kaleb J. Henry